http://researchcommons.waikato.ac.nz/

Research Commons at the University of Waikato

Copyright Statement:

The digital copy of this thesis is protected by the Copyright Act 1994 (New Zealand).

The thesis may be consulted by you, provided you comply with the provisions of the Act and the following conditions of use:

- Any use you make of these documents or images must be for research or private study purposes only, and you may not make them available to any other person.
- Authors control the copyright of their thesis. You will recognise the author's right to be identified as the author of the thesis, and due acknowledgement will be made to the author where appropriate.
- You will obtain the author's permission before publishing any material from the thesis.

Comparison of Wave and Turbulence Evolution in Magnetohydrodynamics

A thesis

submitted in fulfillment

of the requirements for the Degree

of

Master of Science (Research) in Mathematics

at

The University of Waikato

by

Hamish McAlley

THE UNIVERSITY OF
WAIKATO
Te Whare Wānanga o Waikato

2023

Abstract

Magnetohydrodynamics (MHD) is the area of physics dedicated to the study of electrically conducting fluids. These fluids can support linear waves and non-linear turbulence dynamics. This thesis presents results and analysis of the evolution of the linearised MHD equations and the full non-linear MHD equations, starting from the same initial state. A systematic parameter study is conducted, varying the mean magnetic field strength, cross helicity, and Alfvén ratio. The focus is on incompressible MHD, though compressible systems also exist, and indeed are more prevalent as incompressible MHD is largely idealised.

Acknowledgements

To my supervisor, Prof. Sean Oughton, for his patience and expertise. His guidance helped me to take the tools I already possessed for solving differential equations and other methods and apply them to the as yet unknown to me problems covered within the pages of this thesis. Additionally I have come to expand my general knowledge both on the topic and in the broader computer sciences through what Prof. Oughton has taught me when working with large datasets and different systems.

And to my partner Reese, for her unwavering belief in my abilities, which on more than one occasion served as a source of motivation to continue when problems surfaced that seemed to completely derail the train of progress.

Contents

Chapter 1

Introduction

1.1 Background

1.1.1 An Introduction to Magnetohydrodynamics

When an electrically conductive fluid moves, the motions of this fluid produce an electromagnetic field. This field subsequently induces electric currents in the fluid. The combined effect of the magnetic and electric fields give rise to forces which alter the motion of the fluid, including waves and turbulence. This combination electromagnetic-hydrodynamic wave was first described by Swedish physicist Hannes Alfvén in Alfvèn [1942], for which he would eventually receive the Nobel Prize in physics in 1970. These waves would later be dubbed "magnetohydrodynamic waves" [Alfvén, 1946].

Magnetohydrodynamics (MHD) is the study of the dynamics of these electrically conductive fluids in the presence of magnetic fields. These fluids can range from astrophysical plasmas such as the solar wind to liquid metals.

The movement of a conducting fluid has associated electric currents $\boldsymbol{j}$. These electric currents induce (or alter) the magnetic field $\boldsymbol{B}$, but the Lorentz force acting on the fluid due to the $\boldsymbol{j} \times \boldsymbol{B}$ combination of these two fields serves in turn to alter the motion of the fluid, which by Lenz's law will be as to oppose the changes which caused it to move in the first place. This effect shows us that there is some interaction between the velocity and magnetic

fields. The moving conductive fluid can alter the magnetic field, and in turn the magnetic field can produce motion in the fluid. The interaction of these two effects can be quantified using the magnetic Reynolds number $R_m = \frac{UL}{\eta}$, which increases with greater typical velocity U and typical length scales L of the flow, and decreases with greater magnetic diffusion (η). For liquid metals (e.g. mercury, gallium) R_m is typically very small and the interaction weak, whereas in plasmas it is usually large and the interaction is much stronger [Galtier, 2016].

1.2 My Research

The MHD equations support linearised wave motions and also strongly non-linear turbulence. At large mechanical and magnetic Reynolds numbers both waves and turbulence are likely to be present. The evolution of a system of linear waves will be quite different to the non-linear evolution that starts from the same initial state. In this project I use numerical simulations to explore these two situations, and compare how they evolve under a variety of initial conditions.

Chapter 2

The MHD Equations

2.1 The Ideal MHD Equations

MHD fluids are described by a combination of Maxwell's Equations with the hydrodynamic equations in which the Lorentz force is relevant. To begin with we ignore the dissipative effects of viscosity (ν) and resistivity (η). In SI units these equations are:

Gauss' Law

$$\nabla \cdot \boldsymbol{E} = \frac{\rho_c}{\varepsilon_0} \tag{2.1}$$

Gauss' Law for magnetism

$$\nabla \cdot \boldsymbol{B} = 0 \tag{2.2}$$

Maxwell-Faraday equation

$$\nabla \times \boldsymbol{E} = -\frac{\partial \boldsymbol{B}}{\partial t} \tag{2.3}$$

Maxwell's revision of Ampere's Law

$$\nabla \times \boldsymbol{B} = \mu_0 \left(\boldsymbol{J} + \varepsilon_0 \frac{\partial \boldsymbol{B}}{\partial t} \right) \tag{2.4}$$

Where $\boldsymbol{E}$ is the electric field, ρ_c the charge density, ε_0 the permittivity of free space, $\boldsymbol{B}$ the magnetic field, μ_0 the permeability of free space, and $\boldsymbol{J}$ the electric current density [Galtier, 2016]. Note, however, that in the non-relativistic limit to which MHD belongs, the displacement current is, in fact,

negligible. This reduces equation (2.4) to

$$\nabla \times \boldsymbol{B} = \mu_0 \boldsymbol{J} \tag{2.5}$$

Of particular interest to us are the Maxwell-Faraday equation (2.3) and Ampere's law (2.5) alongside Gauss' magnetic divergence constraint (2.2). Taking equation (2.3) in conjunction with Ohm's Law

$$\boldsymbol{E} + \boldsymbol{v} \times \boldsymbol{B} = 0 \tag{2.6}$$

(where $\boldsymbol{v}$ is the velocity) gives us an equation for the magnetic field in MHD:

$$\frac{\partial \boldsymbol{B}}{\partial t} = \nabla \times (\boldsymbol{v} \times \boldsymbol{B}) \tag{2.7}$$

Now consider the momentum equation with mass density ρ and pressure p:

$$\rho \left(\frac{\partial}{\partial t} + \boldsymbol{v} \cdot \nabla \right) \boldsymbol{v} = \boldsymbol{J} \times \boldsymbol{B} - \nabla p \tag{2.8}$$

We know from equation (2.5) that $\boldsymbol{J} = \frac{\nabla \times \boldsymbol{B}}{\mu_0}$, and using the vector identity $\frac{1}{2}(\boldsymbol{B} \cdot \boldsymbol{B}) = (\boldsymbol{B} \cdot \nabla)\boldsymbol{B} + \boldsymbol{B} \times (\nabla \times \boldsymbol{B})$, we thus find that $\boldsymbol{J} \times \boldsymbol{B}$ can, in fact, be expressed as

$$\boldsymbol{J} \times \boldsymbol{B} = \frac{(\boldsymbol{B} \cdot \nabla)\boldsymbol{B}}{\mu_0} - \nabla \left(\frac{B^2}{2\mu_0} \right) \tag{2.9}$$

From this we obtain:

$$\rho \left(\frac{\partial}{\partial t} + \boldsymbol{v} \cdot \nabla \right) \boldsymbol{v} = -\nabla \left(p + \frac{B^2}{2} \right) + \frac{(\boldsymbol{B} \cdot \nabla)\boldsymbol{B}}{\mu_0} \tag{2.10}$$

Finally, we also make use of the mass continuity equation:

$$\frac{\partial \rho}{\partial t} + \nabla \cdot (\rho \boldsymbol{v}) = 0 \tag{2.11}$$

Equations (2.2), (2.7), (2.10), and (2.11) therefore give us the equations that govern ideal (dissipationless) magnetohydrodynamic systems:

$$\boxed{\begin{aligned} \rho \left(\frac{\partial}{\partial t} + \boldsymbol{v} \cdot \nabla \right) \boldsymbol{v} &= -\nabla \left(p + \frac{B^2}{2} \right) + \frac{(\boldsymbol{B} \cdot \nabla)\boldsymbol{B}}{\mu_0} \\ \frac{\partial \boldsymbol{B}}{\partial t} &= \nabla \times (\boldsymbol{v} \times \boldsymbol{B}) \\ \frac{\partial \rho}{\partial t} + \nabla \cdot (\rho \boldsymbol{v}) &= 0 \\ \nabla \cdot \boldsymbol{B} &= 0 \end{aligned}}$$

2.2 Waves and Dispersion Relations

2.2.1 Incompressible

Let us consider first the case of an incompressible fluid with no disspation. In such a case we find that the divergence of the velocity field, $\nabla \cdot \boldsymbol{v}$, is equal to zero, and coupled with the fact that the same can be said for the divergence of the magnetic field, $\nabla \cdot \boldsymbol{B}$, we are able to make use of a simplified version of equation (2.7), that which governs the magnetic field. We assume as well a uniform mass density $\rho = \rho_0 =$ some constant.

To present this equation in a more symmetric way, we can make use of the vector identity:

$$\nabla \times (\boldsymbol{v} \times \boldsymbol{F}) = ((\nabla \cdot \boldsymbol{F}) + \boldsymbol{F} \cdot \nabla)\, \boldsymbol{v} - ((\nabla \cdot \boldsymbol{v}) + \boldsymbol{v} \cdot \nabla)\, \boldsymbol{F}$$

Applying this to the relevant fields $\boldsymbol{v}$ and $\boldsymbol{B}$ and with a little simplification we find that equation (2.7) can in this case be represented using

$$\frac{\partial \boldsymbol{B}}{\partial t} + \boldsymbol{v} \cdot \nabla \boldsymbol{B} = \boldsymbol{B} \cdot \nabla \boldsymbol{v} \tag{2.12}$$

Suppose $\boldsymbol{B}$ is composed of two pieces, a uniform part $\boldsymbol{B}_0$ and fluctuations $\boldsymbol{B}'$. We can find a frame of reference in which the uniform magnetic field can be expressed as $\boldsymbol{B}_0 = B_0 \boldsymbol{e}_{||}$, where $\boldsymbol{e}_{||}$ is a Cartesian unit vector. For ease of notation, we can define a normalised form of this magnetic field as $\boldsymbol{b}_0 \equiv \frac{\boldsymbol{B}_0}{\sqrt{\mu_0 \rho_0}}$ and thus the total magnetic field can be represented as the combination of $\boldsymbol{b} + \boldsymbol{b}_0$ where $\boldsymbol{b} = \frac{\boldsymbol{B}'}{\sqrt{\mu_0 \rho_0}}$. $\boldsymbol{b}_0$ is usually referred to as the Alfvénspeed and is one of the characteristic wave speeds in MHD. This gives us the system of simplified equations:

$$\frac{\partial \boldsymbol{v}}{\partial t} + \boldsymbol{v} \cdot \nabla \boldsymbol{v} = -\nabla \left(\frac{P}{\rho_0} + (\boldsymbol{b} + \boldsymbol{b}_0)^2 \right) + (\boldsymbol{b} + \boldsymbol{b}_0) \cdot \nabla \boldsymbol{b} \tag{2.13}$$

$$\frac{\partial \boldsymbol{b}}{\partial t} + \boldsymbol{v} \cdot \nabla \boldsymbol{b} = (\boldsymbol{b} + \boldsymbol{b}_0) \cdot \nabla \boldsymbol{v} \tag{2.14}$$

$$\nabla \cdot \boldsymbol{v} = \nabla \cdot \boldsymbol{b} = 0 \tag{2.15}$$

Upon revision of the above equations, in particular equation (2.13), we can apply the divergence operator and see that the pressure of the system is depen-

dant only on the non-linear terms. The linearisation of the system is therefore not affected by the pressure, which can thus be ignored in the process (see Appendix A). This leaves us with the following linearised equations, still subject to the divergence zero condition (equation (2.15))

$$\frac{\partial \boldsymbol{v}}{\partial t} = \boldsymbol{b}_0 \cdot \nabla \boldsymbol{b} \tag{2.16}$$

$$\frac{\partial \boldsymbol{b}}{\partial t} = \boldsymbol{b}_0 \cdot \nabla \boldsymbol{v} \tag{2.17}$$

Taking $\boldsymbol{e}_{||}$ parallel to the Cartesian z-direction, the right hand sides of equations (2.16) and (2.17) become $b_0 \frac{\partial \boldsymbol{b}}{\partial z}$ and $b_0 \frac{\partial \boldsymbol{v}}{\partial z}$, respectively. To find the dispersion relation from here we use the Fourier decompositions:

$$\hat{\boldsymbol{v}} = \boldsymbol{v}_1 e^{i(\boldsymbol{k}\cdot\boldsymbol{z} - \omega t)}, \qquad \hat{\boldsymbol{b}} = \boldsymbol{b}_1 e^{i(\boldsymbol{k}\cdot\boldsymbol{z} - \omega t)}$$

where $\boldsymbol{v}_1$, $\boldsymbol{b}_1$ are complex-valued and it is understood that only the real parts of the right hand side are to be used. Additionally, $\boldsymbol{k}$ and ω are known as the Fourier wave vector and the Fourier angular frequency. Applying these to the linearised system gives us the following equivalents:

$$\frac{\partial \hat{\boldsymbol{v}}}{\partial t} = i b_0 k_z \hat{\boldsymbol{b}}$$

$$\frac{\partial \hat{\boldsymbol{b}}}{\partial t} = i b_0 k_z \hat{\boldsymbol{v}}$$

which, with just a small amount of simplification, becomes

$$\omega \boldsymbol{v}_1 = -b_0 k_z \boldsymbol{b}_1 \tag{2.18}$$

$$\omega \boldsymbol{b}_1 = -b_0 k_z \boldsymbol{v}_1 \tag{2.19}$$

Combining these equations and simplifying gives us the solution for the dispersion relation of incompressible MHD waves:

$$\omega^2 = (b_0 k_z)^2 = (\boldsymbol{k} \cdot \boldsymbol{b}_0)^2 \tag{2.20}$$

The associated waves are called the Alfvén waves. These Alfvén waves were predicted by Alfvén in his 1942 paper [Alfvèn, 1942] though they were not experimentally verified until Allen et al. [1959], who were able to generate such

waves under laboratory conditions in a cylindrical plasma, and subsequently detect the transmitted waves at the other end. They were able to calculate the velocity of the transmitted waves and found that they came out to be somewhat higher than predicted, though to within the extent expected due to their conditions. This overestimate is born out of the methodology of the experiment and the preionisation of the tube in which the waves were produced. Exact details are covered in the paper itself, though they are surplus to the scope of this thesis. The results themselves can be seen in figure 2.1

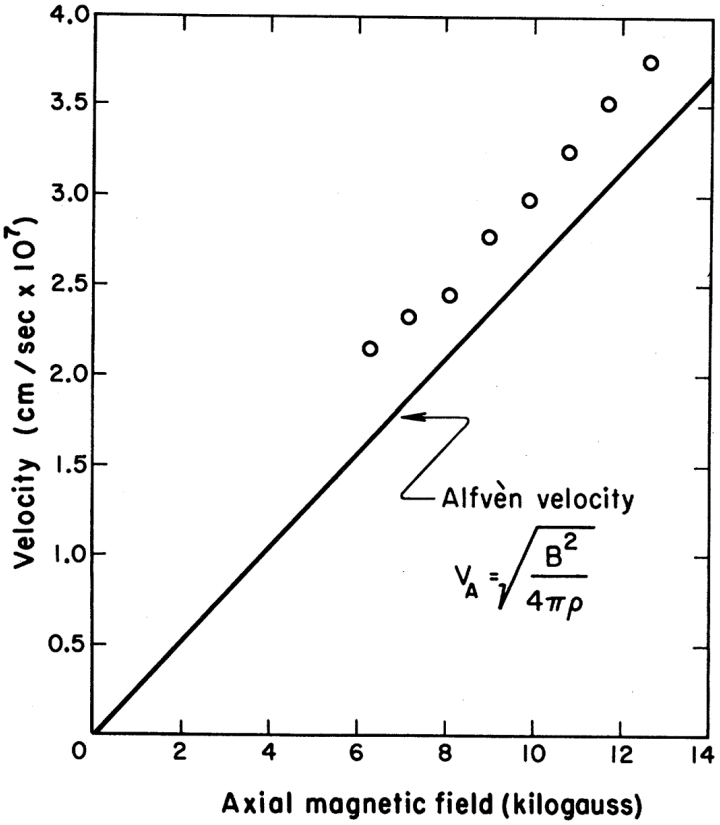

Figure 2.1: Velocity of the waves vs magnetic field. The points represent the values of the generated waves, while the solid line is the theoretical value for the Alfvén wave. Image credit: Allen et al. [1959]

2.2.2 Compressible MHD

We will now take the case of compressible MHD assuming the polytropic pressure equation

$$P = A\rho^{\gamma} \tag{2.21}$$

Using a similar Fourier decomposition as used in the incompressible case, e.g. $\hat{\rho} = \rho_1 e^{i(\boldsymbol{k}\cdot\boldsymbol{z}-\omega t)}$, we can now obtain the following linearised system for polytropic compressible MHD:

$$\omega \boldsymbol{v}_1 = \boldsymbol{k}\left(A\gamma\rho_0^{\gamma-2}\rho_1 - \boldsymbol{b}_0\cdot\boldsymbol{b}_1\right) - b_0 k_z \boldsymbol{b}_1 \tag{2.22}$$

$$\omega \boldsymbol{b}_1 = -b_0 k_z \boldsymbol{v}_1 + \boldsymbol{b}_0(\boldsymbol{k}\cdot\boldsymbol{v}_1) \tag{2.23}$$

$$\omega \rho_1 = \rho_0 \boldsymbol{k}\cdot\boldsymbol{v}_1 \tag{2.24}$$

By substituting equations (2.23) and (2.24) into equation (2.22) and calling $c_s^2 \equiv A\gamma\rho_0^{\gamma-1}$ the speed of sound, we are able to eliminate ρ_1 and $\boldsymbol{b}_1$ to obtain the following equation for just $\boldsymbol{v}_1$:

$$\begin{aligned}
\omega^2\boldsymbol{v}_1 &= \boldsymbol{k}\left(c_s^2\boldsymbol{k}\cdot\boldsymbol{v}_1 + \boldsymbol{b}_0\cdot\left(-b_0k_z\boldsymbol{v}_1 + \boldsymbol{b}_0\left(\boldsymbol{k}\cdot\boldsymbol{v}_1\right)\right)\right) - b_0k_z\left(-b_0k_z\boldsymbol{v}_1 + \boldsymbol{b}_0\left(\boldsymbol{k}\cdot\boldsymbol{v}_1\right)\right)\\
&= \boldsymbol{k}\left(c_s^2\boldsymbol{k}\cdot\boldsymbol{v}_1 - b_0k_z\boldsymbol{b}_0\boldsymbol{v}_1 + b_0^2\left(\boldsymbol{k}\cdot\boldsymbol{v}_1\right)\right) + (b_0k_z)^2\boldsymbol{v}_1 - b_0k_z\boldsymbol{b}_0(\boldsymbol{k}\cdot\boldsymbol{v}_1)\\
&= \boldsymbol{k}\left(\left(c_s^2+b_0^2\right)\left(\boldsymbol{k}\cdot\boldsymbol{v}_1\right) - (\boldsymbol{b}_0\cdot\boldsymbol{k})(\boldsymbol{b}_0\cdot\boldsymbol{v}_1)\right) + (b_0k_z)^2\boldsymbol{v}_1 - \boldsymbol{b}_0(\boldsymbol{b}_0\cdot\boldsymbol{k})(\boldsymbol{k}\cdot\boldsymbol{v}_1)
\end{aligned}$$

$$\implies \left(\omega^2 - (\boldsymbol{k}\cdot\boldsymbol{b}_0)^2\right)\boldsymbol{v}_1 = \boldsymbol{k}\left[\left(c_s^2+b_0^2\right)\left(\boldsymbol{k}\cdot\boldsymbol{v}_1 - (\boldsymbol{b}_0\cdot\boldsymbol{k})(\boldsymbol{b}_0\boldsymbol{v}_1)\right]\right. - \boldsymbol{b}_0(\boldsymbol{b}_0\cdot\boldsymbol{k})(\boldsymbol{k}\cdot\boldsymbol{v}_1) \tag{2.25}$$

Since we have $\boldsymbol{b}_0$ associated with a preferred direction, it makes sense physically and mathematically to express the wave vector in terms of components in the parallel and perpendicular directions to $\boldsymbol{b}_0$, and as such we can define $\boldsymbol{k} = k_\perp\boldsymbol{e}_x + k_\parallel\boldsymbol{e}_z$ and can therefore obtain the following system:

$$\begin{pmatrix} \omega^2 - k^2b_0^2 - k_x^2c_s^2 & 0 & -c_s^2k_xk_z \\ 0 & \omega^2 - k^2b_0^2 & 0 \\ -c_s^2k_xk_z & 0 & \omega^2 - k_z^2c_s^2 \end{pmatrix}\begin{pmatrix} v_x \\ v_y \\ v_z \end{pmatrix} = \begin{pmatrix} 0 \\ 0 \\ 0 \end{pmatrix} \tag{2.26}$$

This system will have a non-trivial solution if the determinant of the matrix is zero. Considering this condition, we acquire:

$$\left(\omega^2 - k_z^2b_0^2\right)\left(\omega^4 - \left(c_s^2+b_0^2\right)k^2\omega^2 + c_s^2k^2k_z^2b_0^2\right) = 0 \tag{2.27}$$

The first factor of this system immediately gives as a solution the incompressible Alfvén wave already derived previously in section 2.2.1. The second piece is a quadratic equation with respect to ω^2, and can therefore also be easily solved to find:

$$\omega_+^2 = \frac{k^2}{2}\left(c_s^2 + b_0^2 + \sqrt{\left(c_s^2 + b_0^2\right)^2 - \frac{4c_s^2 k_z^2 b_0^2}{k^s}}\right) \tag{2.28}$$

$$\omega_-^2 = \frac{k^2}{2}\left(c_s^2 + b_0^2 - \sqrt{\left(c_s^2 + b_0^2\right)^2 - \frac{4c_s^2 k_z^2 b_0^2}{k^s}}\right) \tag{2.29}$$

Waves travelling with a dispersion relation as in equation (2.28) will propagate faster than the Alfvén waves, whereas waves associated with a dispersion relation as in equation (2.29) will propagate at velocities less than the Alfvén speed. Hence the somewhat simple names: the fast and slow magnetosonic waves.

The derivations in sections 2.1 and 2.2 have been based on those found Galtier [2016].

2.3 Turbulence and the Transfer of Energy Between Scales

Energy within an MHD system can dissipate due to both the viscosity and the resistivity, but this is mostly small without the non-linear effects of turbulence. Turbulence is a phenomenon that occurs on multiple length scales an mediates the transport of energy, mass, and momentum. It is characterised by unsteady fluctuations in the electric and magnetic fields and flows [El-Alaoui et al., 2021]. Primarily, turbulence will transfer energy from larger scales to smaller dissipation scales. These large, energy containing scales drive turbulence into an inertial range, where the energy transfer follows a power law $k^{-5/3}$ for wavenumber k [Frisch, 1995]. In this range, turbulent eddies break down, eventually becoming small enough that the viscous dampening is significant and energy dissipates faster. Due to this dissipation the energy spectrum steepens as the eddies are damped by the viscosity of the fluid. Eddies of

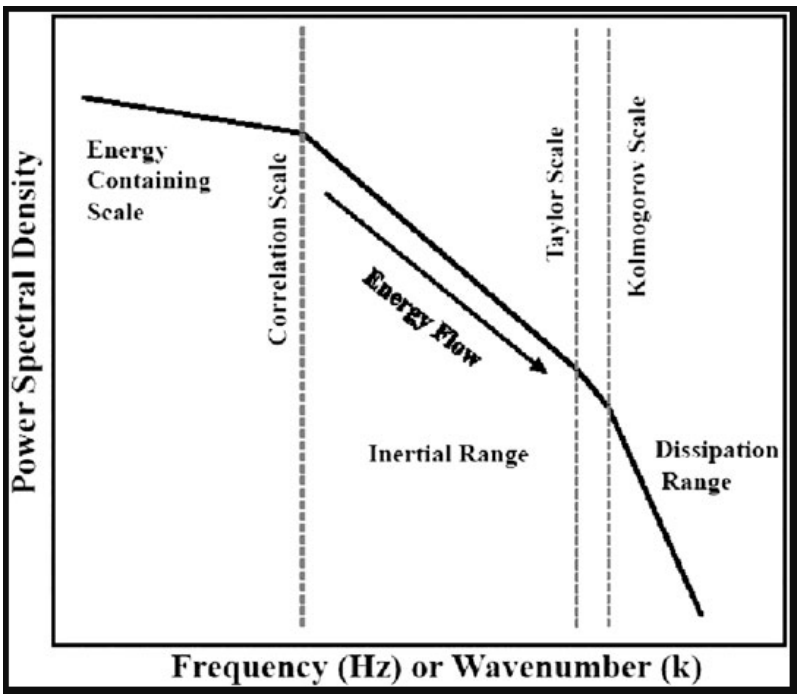

Figure 2.2: A typical power spectral density plot for the solar wind, an example of MHD flow. Image credit: El-Alaoui et al. [2021]

sizes where the dampening effects are important make up what is called the dissipation range. This process is shown in figure 2.2 below.

Chapter 3

Results and Analysis

3.1 Methods

My project is based on a comparison of the evolution of a superposition of linear waves in the linearised MHD system, versus the behaviour of the identical initial set of of fluctuations evolved using the full non-linear 'turbulent' MHD equations.

For the comparison to true non-linear behaviour, data was obtained by running the codes for relevant simulations provided by Professor Sean Oughton, the supervisor of the project and currently involved in similar research of the kind. These simulations provided output data at regular time intervals, including the initial conditions. The data from the initial conditions was used as the initial conditions in my own analysis, which consisted of a linear ordinary differential equation solver in MATLAB which would evolve a solution over time for the magnetic and velocity fields. Over time this solution provided information to calculate values for several variables, which could then be plotted against the corresponding variables from the simulation data to observe any differences between the linear and non-linear models.

Throughout the following analysis I will refer to the outputs of the provided simulation as the "simulation" data, or occasionally the "sim" data where a shorter form is more appropriate, and those of my own analysis as the "solver"

data. Each time data was obtained from a different set of initial conditions, this is referred to as a "run." The full simulations were performed using triply periodic Fourier spectral method codes, with second order Runge-Kutta time stepping. This is essentially equivalent to using a 2π periodic cube discretised into n cells in each Cartesian direction. Values of n employed ranged from $n = 16$ to $n = 512$. Often the value of n used for a particular run is given in the figure titles or captions. Two points of interest were taken as reference points to begin the solving process for my MATLAB solver. Firstly, the initial time $t = 0$ of the simulation run, and secondly the $t = 0.5$ simulation values. The initial time was of interest to see how the two solutions evolve from the same initial parameters, and the $t = 0.5$ point of reference allowed insight into how the solutions diverge if the non-linear terms are given time to have a noticeable effect before being "turned off".

The codes solve the non-dimensionalised MHD equations so that ν and η are really reciprocal mechanical and magnetic Reynolds numbers. Speeds and lengths are in units of U and L, the characteristic values for the flow. Times are in units of $\frac{L}{U}$.

3.1.1 Ideal vs Practical

The equations referenced throughout chapter 2 were theoretical examples used for ideal MHD systems. That is, systems with no viscosity (ν) or electrical resistivity (η). Systems such as these would allow for perfect transmission of energy throughout the system. For testing purposes, I made use of ideal systems in several runs.

Of course, in real systems, these dissipative components do exist, and have the effect of dampening the energy of a closed system over time. Both the simulation and the solver make use of additional terms to take into account both the resistivity and viscosity. For the purposes of this project we set $\nu = \eta$, but this does not necessarily need to be the case in all situations. When the

dissipative components are taken into account, equation (2.6) extends to

$$\boldsymbol{E} + \boldsymbol{v} \times \boldsymbol{B} = \eta \boldsymbol{j} \tag{3.1}$$

and the MHD equations become:

$$\rho \left(\frac{\partial}{\partial t} + \boldsymbol{v} \cdot \nabla \right) \boldsymbol{v} = -\nabla \left(p + \frac{B^2}{2} \right) + \frac{(\boldsymbol{B} \cdot \nabla)\, \boldsymbol{B}}{\mu_0} + \nu \nabla^2 \boldsymbol{v} + \frac{\nu}{3} \nabla (\nabla \cdot \boldsymbol{v}) \tag{3.2}$$

$$\frac{\partial \boldsymbol{B}}{\partial t} = \nabla \times (\boldsymbol{v} \times \boldsymbol{B}) + \eta \nabla^2 \boldsymbol{B} \tag{3.3}$$

$$\frac{\partial \rho}{\partial t} + \nabla \cdot (\rho \boldsymbol{v}) = 0 \tag{3.4}$$

$$\nabla \cdot \boldsymbol{B} = 0 \tag{3.5}$$

3.2 Testing

3.2.1 Single $\boldsymbol{k}$ Vector

I began by first seeing if my MATLAB solver was accurate when it only needed to deal with a single specified value for the wave vector $\boldsymbol{k}$, namely the arbitrary vector $\boldsymbol{k} = (2, 4, 3)$, under ideal conditions and in an incompressible system. Given a specific value for $\boldsymbol{k}$, it is relatively simple to find the solution to the MHD equations analytically. Testing was done using an arbitrary value for $b_0 = 1$. For the chosen vector, we get $k^2 = 29$ and $k_z = 3$.

We know from equations 2.16 to 2.19 and the inclusion of the damping terms $\eta \nabla^2 \boldsymbol{b}$ and $\nu \nabla^2 \boldsymbol{v}$ that we need to solve the coupled system

$$\frac{\partial \boldsymbol{v}}{\partial t} = i b_0 k_z \boldsymbol{b} - \nu k^2 \boldsymbol{v} \tag{3.6}$$

$$\frac{\partial \boldsymbol{b}}{\partial t} = i b_0 k_z \boldsymbol{v} - \eta k^2 \boldsymbol{b} \tag{3.7}$$

which, when ν is allowed to equal η gives us the characteristic polynomial

$$\lambda^2 + 2\eta k^2 \lambda + (k_z b_0)^2 + \eta^2 k^4 = 0 \tag{3.8}$$

From here I tested two possibilities. Firstly, the trivial case where $\eta = \nu = 0$. In this case, equation 3.8 reduces down to $\lambda^2 + (k_z b_0)^2 = 0$ which has

solutions $\lambda = \pm k_z b_0 i$, as was found in section 2.2.1. Given initial conditions of (in Fourier-space) $v_x = 564.97 + 1129.9i$ and $b_x = -v_x$, this leads to solutions

$$v_x = (564.97 + 1129.9i)e^{-3it}$$
$$b_x = -(564.97 + 1129.9i)e^{-3it}$$

which were verified with the solver at all times t. Note that solution oscillates with the appropriate Alfvén wave frequency $\omega = k_z b_0 = 3$.

The second possibility I tested was a slightly more complex case where $\nu = \eta = 0.01$. In this possibility equation 3.8 does not reduce, but we can benefit from recognising the perfect square $(\lambda + \eta k^2)^2 = -(k_z b_0)^2$ which has solutions $\lambda = -0.29 \pm 3i$. Under the same initial conditions as in the trivial case, this gives the solution

$$\begin{pmatrix} v_x \\ b_x \end{pmatrix} = (564.97 + 1129.9i)e^{(-0.29-3i)t} \begin{pmatrix} 1 \\ -1 \end{pmatrix}$$

which, once again, was successfully produced by the solver and verified for all times t. These solutions correspond to damped oscillations of an Alfvén wave.

3.2.2 Colinear $\boldsymbol{k}$ Vectors

Having established that my solver was able to accurately produce a solution for each value of the vector $\boldsymbol{k}$ individually, the next step was to determine if it would continue to be accurate for a series of different values excited at once. The solver is designed to evolve a solution to the MHD equations as though they were linear only, and as such for this test case the simulation was initialised to match. The MHD equations become linear if all the excited Fourier modes have $\boldsymbol{k}$'s which are parallel, as this condition makes the values of $\boldsymbol{v} \cdot \nabla \boldsymbol{v}$ and $\boldsymbol{b} \cdot \nabla \boldsymbol{b}$ zero. Thus, only select $\boldsymbol{k}$ vectors were excited to produce a linear evolution of wave-only behaviour. The particular colinear $\boldsymbol{k}$'s used for this case were the scalar multiples of $\boldsymbol{k} = (2, 3, 4)$, that is $\alpha \times (2, 3, 4)$ for $\alpha = 1, 2, 3...$ Fig 3.1 shows the kinetic and magnetic energy plots over time for three different cases of this colinear set up for $\boldsymbol{k}$.

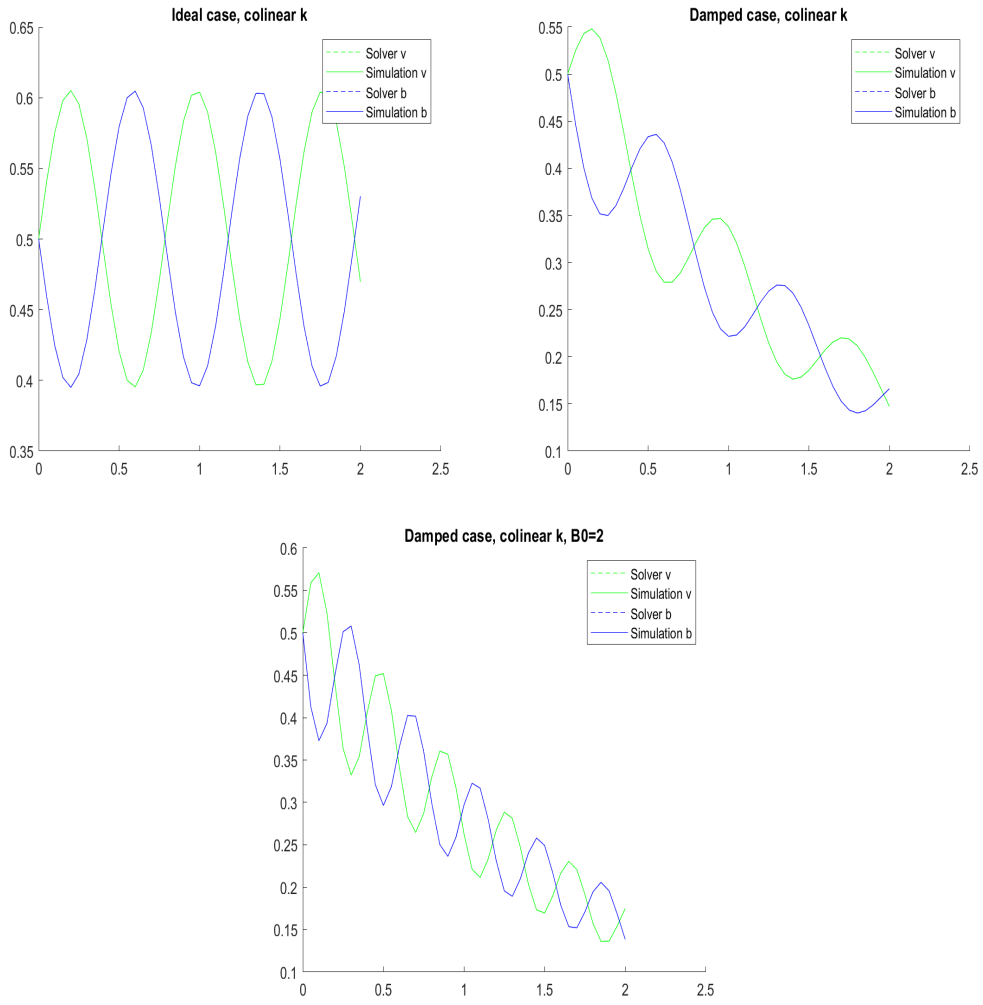

Figure 3.1: Plotting the kinetic (in green) and magnetic (in blue) energies of an MHD system in which the excited $\boldsymbol{k}$ vectors in Fourier space lead to a linear evolution. Values are normalised so that along the x-axis the time is measured in units of nominal non-linear times and the y-axis is measured in units of the initial energy levels. For these tests I used $n = 32$

The first plot shows the energy levels for an ideal MHD fluid, where the viscosity and resistivity are zero, and therefore the energy does not dissipate over time. This is shown clearly in the first plot where the energy oscillates according to the solution to the linearised equations, but the mean line, which travels through the centre of the oscillations, does not diverge from the mean value of 0.5. This is the simplest case of the colinear system and, as evidenced by the total overlap of the dotted and solid lines in the plot, my solver was

able to replicate the same values exactly.

The second plot shows the same energy levels, but now the system is non-ideal and the viscosity and resistivity do have a dampening effect on the total energy as time moves forward. The oscillation due to the wave activity remains, though now as time passes the total energy in the system decreases.

The third plot shows the results of the system under the same dampening conditions, though now the strength of the magnetic field has been doubled. This was done to test that my solver was appropriately using the value of the magnetic field to make sure that it was not restricted to just as single case. A greater magnetic field strength should lead to increased oscillation frequency, which is the effect that shows on the graph.

In all three cases, my solver obtained an output that perfectly matched the solution of the simulation. Fig 3.2 shows this match more clearly for three runs with distinct values of σ_c, but otherwise the same parameters. Here, the solver solutions are highlighted using symbols, showing clearly the overlap between solver and simulation solutions.

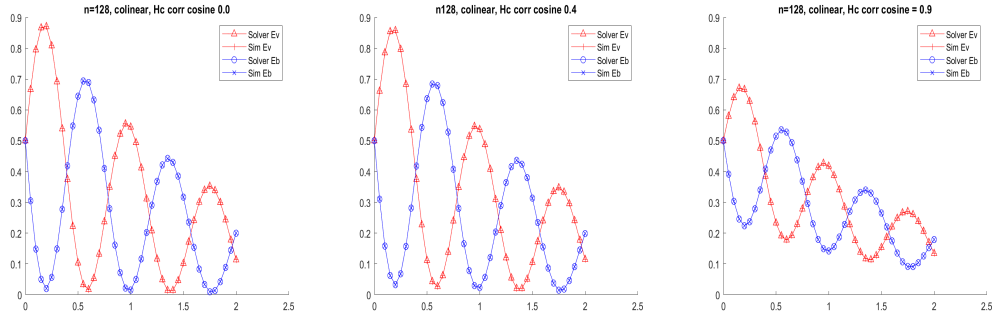

Figure 3.2: As the normalised cross helicity increases, the amplitude of the oscillations in the solution to the colinear system decreases, because of the reducing fraction of counter-propagating waves.

With multiple different system parameters and initial conditions being solved accurately by my solver, I could now move on to finding solutions to systems with more realistic physical parameters where many non-colinear wave vectors $\boldsymbol{k}$ are excited.

3.3 Incompressible Case

3.3.1 Elsässer Variables

Of a special interest to solving the MHD equations in the incompressible case are the so-called Elsässer variables. These are a simple transformation proposed by Walter Elsässer [1950] involving the sums and differences of the magnetic and velocity fields with the magnetic field in Alfvén units, i.e. $\boldsymbol{b} = \frac{\boldsymbol{B'}}{\sqrt{\mu_0 \rho_0}}$. Much like our original magnetic field they can be normalised in the same way and can thus be defined as

$$\boldsymbol{z}^{\pm} \equiv \boldsymbol{v} \pm \boldsymbol{b} \tag{3.9}$$

The convenience of the Elsässer variables is that they allow us to rewrite the MHD equations:

$$\nabla \cdot \boldsymbol{z}^{\pm} = 0 \tag{3.10}$$

$$\frac{\partial \boldsymbol{z}^{+}}{\partial t} - \boldsymbol{b}_0 \cdot \nabla \boldsymbol{z}^{+} + \boldsymbol{z}^{-} \cdot \nabla \boldsymbol{z}^{+} = -\nabla P_* + \nabla^2(\nu_+ \boldsymbol{z}^{+} + \nu_- \boldsymbol{z}^{-}) \tag{3.11}$$

$$\frac{\partial \boldsymbol{z}^{-}}{\partial t} + \boldsymbol{b}_0 \cdot \nabla \boldsymbol{z}^{-} + \boldsymbol{z}^{+} \cdot \nabla \boldsymbol{z}^{-} = -\nabla P_* + \nabla^2(\nu_- \boldsymbol{z}^{+} + \nu_+ \boldsymbol{z}^{-}) \tag{3.12}$$

where the dissipative terms are $\nu_{\pm} = \frac{1}{2}(\nu \pm \eta)$. It turns out that in the incompressible case, either of $\boldsymbol{z}^{\pm} = 0$ can be a solution, in which case the other Elsässer field will evolve linearly. More generally, the ideal linearised problem can be reduced, in Fourier space and in the same manner as in section 2.2.1, to:

$$\frac{\partial \boldsymbol{z}^{\pm}}{\partial t} = \pm i k_z b_0 \boldsymbol{z}^{\pm} \tag{3.13}$$

This simplification, along with the simple reverse transform to take the Elsässer variables and return them to the magnetic and velocity fields, allowed for a simpler computation for my MATLAB solver to apply.

3.3.2 Solutions

To investigate as thoroughly as possible what effects the presence or absence of turbulence has on the evolution of an initial set of MHD waves, I tested for a variety of initial conditions. The factors which varied across runs were:

- the initial Alfvén ratio $r_A = \frac{E_v}{E_b}$, tested at values 0.5, 1.0, and 2.0
- the initial normalised cross helicity $\sigma_c = \frac{\langle \boldsymbol{v} \cdot \boldsymbol{b} \rangle}{E_v + E_b}$, tested at values 0.0, 0.4, and 0.9
- the strength of the uniform magnetic field b_0, tested at values of 1.0 and 2.0

For $b_0 = 2.0$, only the Alfvén ratio $r_A = 1.0$ was used. In addition to the energy levels and cross helicity over time, it is also of interest to see the contribution of different values of $\boldsymbol{k}$ as well, that is to plot the various spectra. The specific contribution was calculated for each $\boldsymbol{k}$ and grouped in 'shells' according to the magnitude k.

Magnetic Field Strength $b_0 = 1.0$

A most basic case is that with initial conditions $\sigma_c = 0.0$ and $r_A = 1.0$. Fig 3.3 shows the major results of this run compared to time when the reference point is taken as the initial time $t = 0$, and fig 3.4 shows the various energy spectra for the same conditions.

We can clearly see that in the case of the solver, where turbulence is absent, there is a roughly linear decrease in energy levels. In this situation there is no transfer of energy between wave vector modes. However in the case of the simulation data, where the system is turbulent, we see the kinetic energy decrease much more rapidly as the non-linear dynamics transfers energy to smaller scales (larger $\boldsymbol{k}$'s). Initially, the drop in magnetic energy is slower than that of the kinetic energy, however after $t \approx 0.3$ it also begins to dissipate much faster than in the linear system.

The plots for ω^2 and j^2 are notable in that the constant decrease seen in the linear system is not matched by the turbulent system. In fact, in the turbulent system we see an initial increase in these values, peaking at $t \approx 0.4$ before dropping off rapidly, in tandem with the decrease in energy. In both systems we see an expected decrease in the cross helicity as the overall energy levels

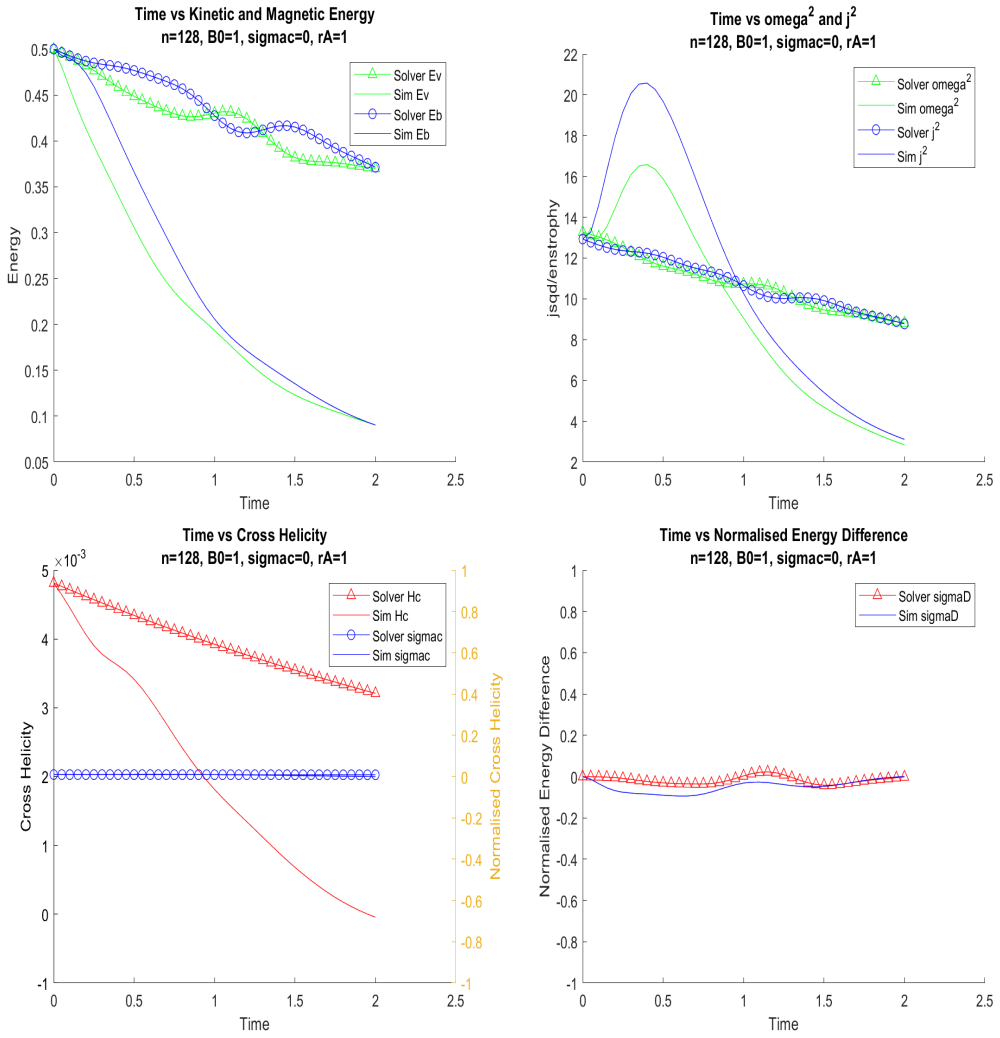

Figure 3.3: Time plots for the various energy measures in the run of $n = 128$, $b_0 = 1.0$, $\sigma_c = 0.0$, $r_A = 1.0$ beginning from t=0

decrease. Once again the decrease is much stronger for the turbulent system where the energy cascade to smaller scales leads to more efficient dissipation. It is worth noting though that the scale of this activity is very small, only around 10^{-3}. The normalised cross helicity in the linear system decreases at a very slow, almost negligible rate, owing to the relatively small drop in overall energy over the timespan. The normalised energy difference, $\sigma_D = \frac{E_v - E_b}{E_v + E_b}$, is much the same between the two systems, with the simulation values being lower at almost all points, corresponding to the lag we saw in the reduction of magnetic energy. Fluctuations overall are small however, so really there is nothing of note.

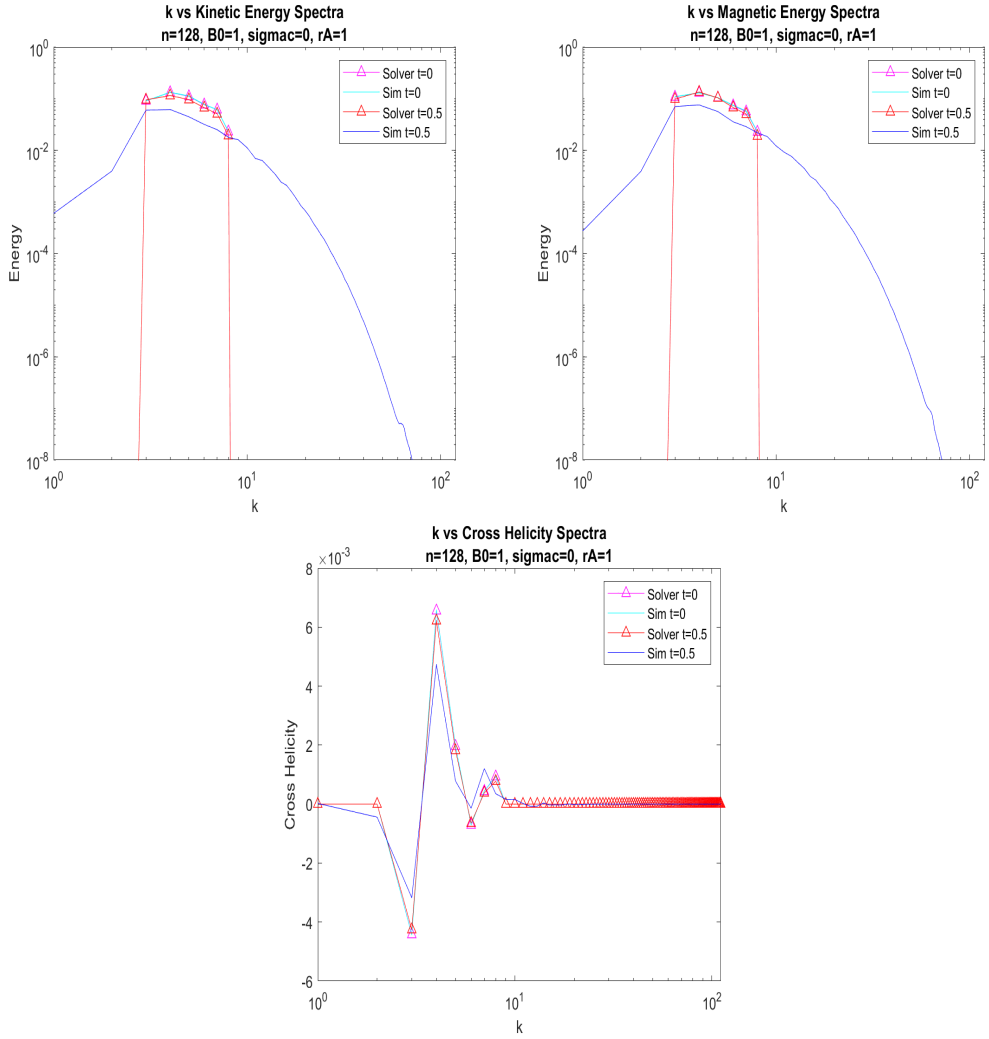

Figure 3.4: Spectra plots for the energy measures in the run of $n = 128$, $b_0 = 1.0$, $\sigma_c = 0.0$, $r_A = 1.0$, where the solver takes its initial reference as t=0. The evolution at t=0.5 is also plotted

In the case of the energy spectra, initially all the energy is restricted to the wave number band $3 < k < 8$, as was set by the initial conditions of each run. Initially, the solver values are a match for those of the simulation. This is to be expected as here the two systems have identical starting states. However as the solution is evolved forward in time to t=0.5 the differences become clear. Whereas the energy spectra for the solver solution remain restricted to the same wave numbers $3 < k < 8$, in the simulation the energy has spread out to other shells. This is a result of the non-linear effects transferring energy into smaller scales and thus spreading it over larger wavenumber bands associated

with larger k's. We see this as well in the fact that the total amount of energy is also much lower in the simulation. The spread of energy to smaller scales allows for a more efficient dissipation and so the overall energy levels decrease much faster.

We can see that while the cross helicity is initially a match between the MATLAB solver and the simulation, as is expected. What we see as the systems evolve however is that for the linear system there is almost no change from the initial values. There is a very small reduction in the overall cross helicity, but significantly less than there is for the non-linear system. We see a small amount of spread to wavenumber bands outside the initial $3 < k < 8$ as the kinetic and magnetic energy spread, though the scale remains very small.

In fig 3.5 we see the same initial conditions, although this time the solution was allowed to evolve in the simulation until t=0.5 before the MATLAB solver was used. The simulation data plotted is the same as in figure 3.3, but now the evolution of the linear system is plotted beginning at t=0.5. It is clear to see that once the non-linear dynamics from the turbulent system are removed, the energy dissipation slows down to the same rate as in the t=0 start case. Total energy levels are noticeably lower, but this is due to the fact that the conditions with which the MATLAB solver began used the lower energy levels of the already evolved turbulent solution.

For ω^2 and j^2 however, the behaviour does change from the first run. Whereas initially we saw a linear decrease, this decrease is now faster for earlier times. Both ω^2 and j^2 decrease rapidly immediately following their initial state (with j^2 even decreasing faster than in the simulation), before decreasing more slowly as time extends out towards t=2.5. For the cross helicity and its normalisation, as well as the normalised energy difference, we see much the same behaviour from here as we did from the t=0 start case. As in the energy, H_c was able to reach lower overall levels, but once again this is more due to the fact that it started from a lower level than any new behaviour, and once again the scale is small enough as to not be noteworthy.

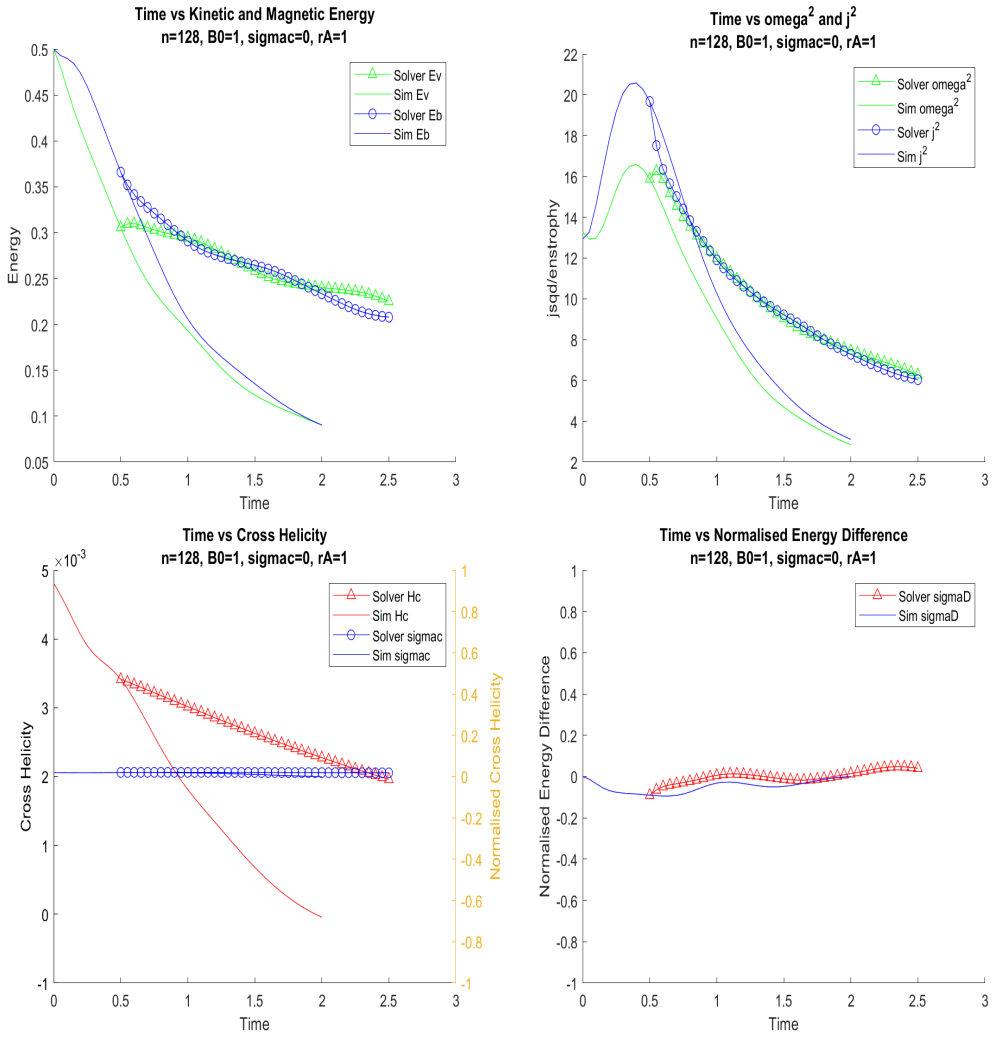

Figure 3.5: Time plots for the various energy measures in the run of $n = 128$, $b_0 = 1.0$, $\sigma_c = 0.0$, $r_A = 1.0$ beginning from t=0.5

Fig 3.6 shows the accompanying spectra graphs to fig 3.5, with values plotted at times t=0.5 and t=1 for both systems, with the addition of the t=0 simulation values for reference. There is a strong match between the "initial" t=0.5 values for the kinetic energy spectra. There is an unexpected difference in the higher k bands between the MATLAB solver and simulation values, though on a very small scale. As the systems progress to t=1 we see the energy levels of the simulation are more spread out as the non-linear action has continued and so the energy has continued to be transferred between wavevector modes. In the case of the solver, it is only linear action happening at this point so there is no further transfer of energy to higher k's. Since it

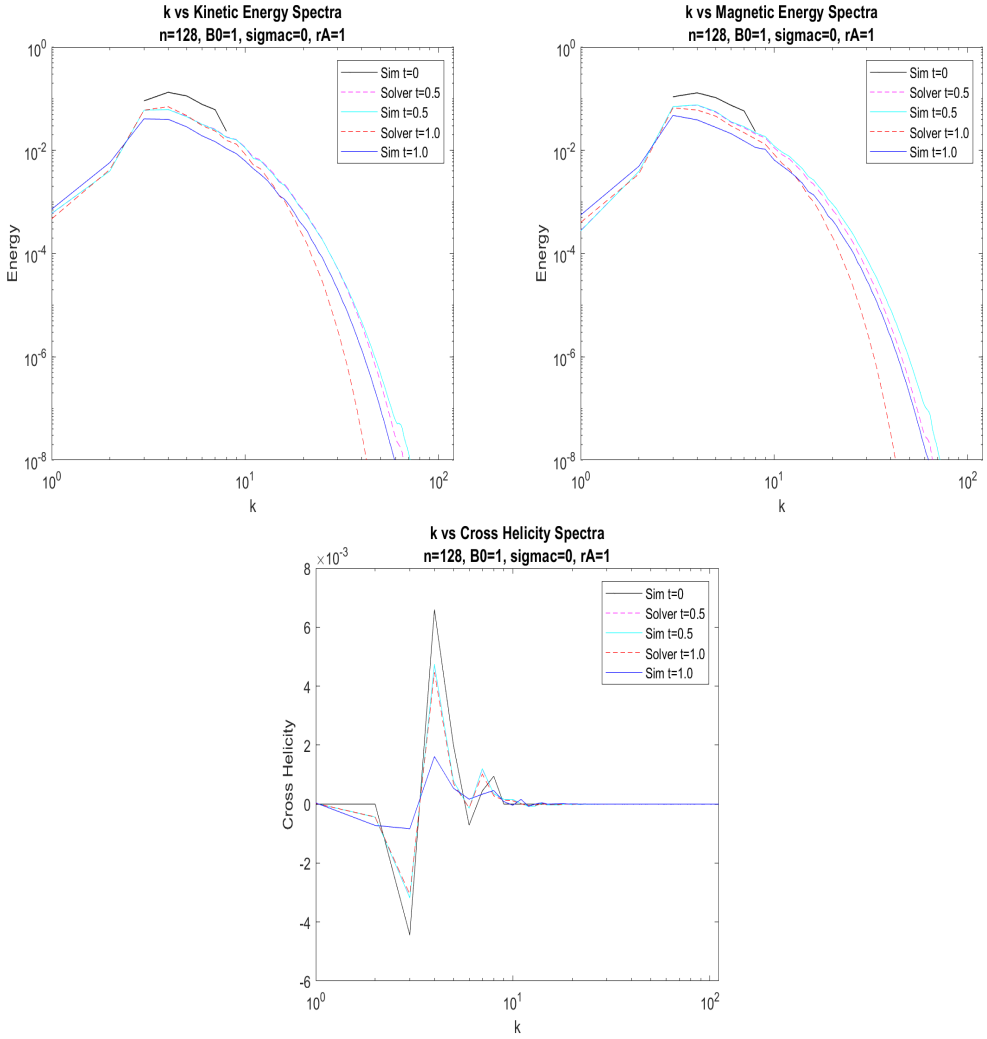

Figure 3.6: Spectra plots for the energy measures in the run of $n = 128$, $b_0 = 1.0$, $\sigma_c = 0.0$, $r_A = 1.0$, where the solver takes its initial reference as t=0.5. The simulation values at t=0 are also plotted

is only the non-linear effects which lead to transfer of energy to the smaller scales, once they are "turned off" this spread was no longer possible. Without the continued transfer of energy from the smaller k's, energy dissipates in the higher bands due to the resistivity and viscosity. As the strength of the dissipation increases quadratically with k, and the non-linear dynamics allow for the energy in higher k's to be replenished due to transfer from larger scales, this leads to lower energy levels in the linear system at these higher wavenumber bands. In the central k band associated with the initial conditions however we see the opposite effect. Dissipation due to viscosity and resistivity

is much lower at the more energetic scales, and for the linearised solutions this is the only way the total energy, $E(k) = E_v(k) + E_b(k)$, can decrease, so we see that there is almost no change from the t=0.5 state. However in the simulation, the non-linear terms result in a net transfer of energy to larger k's and a much larger (non-dissipative) loss of energy from the central band.

The case for the magnetic energy spectra is largely the same, although there is a significant unexpected discrepancy in the t=0.5 values. As with the kinetic energy spectra, this discrepancy is largest at higher values of k. Unfortunately, I was unable to identify any reasons for these differences.

The cross helicity spectra shows almost no change from t=0.5 to t=1 for the MATLAB solver results. Just as in the t=0 start case, the lack of non-linear activity results in a near total lack of change in the cross helicity values. This comes down to the lack of change in the magnetic and particularly the kinetic energies between these times for the same k's. In contrast, the results from the simulation show H_c decreasing at almost all points as time passes. The only exception to this is in the wavenumber bands associated with k's smaller than those used in the initial conditions, as energy is transferred to them from the central band. Everywhere else, as the energy decreases, so does H_c.

Figure 3.7 shows the energy and helicity plots where initial $\sigma_c = 0.0$ and $r_A = 2.0$. As expected with the change in initial conditions, a clear difference is seen at first for the energy. Kinetic energy begins at a value of $\frac{2}{3}$, compared to $\frac{1}{3}$ for the magnetic energy. This is reflective of the Alfvén ratio, so the result is unsurprising. Values for the MATLAB solver very quickly fall back to the small oscillations seen previously, though overall the values remain slightly higher at any given time than for when initial $r_A = 1.0$. For the simulation values, in contrast to the monotonic decrease in magnetic energy for the $r_A = 1.0$ case, here we see an increase at first until a peak near $t \approx 0.3$ before decreasing from there. By $t = 0.5$, the energy levels have reached the same values as they had at this time in the $r_A = 1.0$ case. For enstrophy and j^2 we see a similar

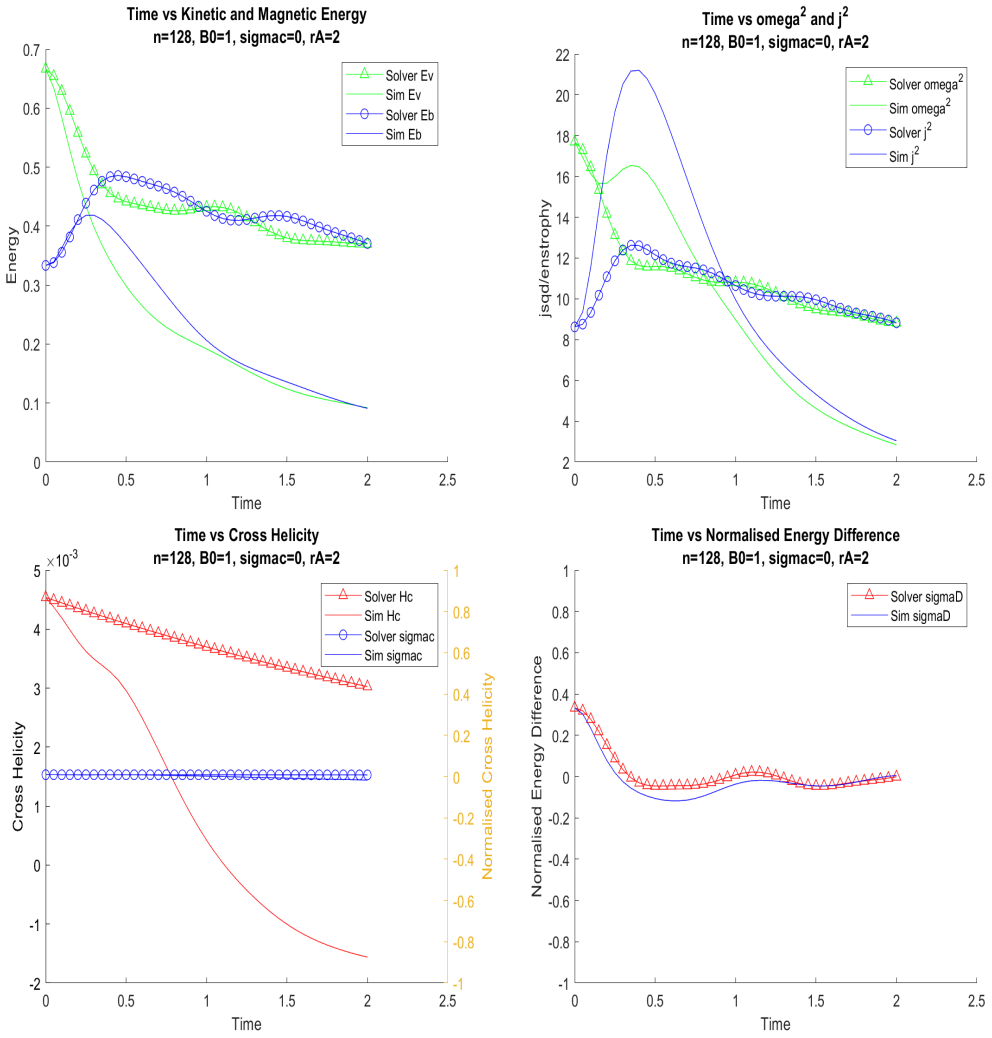

Figure 3.7: Time plots for the various energy measures in the run of $n = 128$, $b_0 = 1.0$, $\sigma_c = 0.0$, $r_A = 2.0$ beginning from t=0

story. They begin with values very far apart but quickly return to the small oscillations we saw previously. In this case however the oscillations do retain a slightly larger amplitude. Cross helicity remains almost identical for the MATLAB solver as the Alfvén ratio changes, starting slightly lower – though not significantly so – and diminishing at the same rate. For the simulation, while the shape remains the same, the decrease in cross helicity decreases much faster, ending up noticeably lower by the end point of the run. For both systems however the normalised cross helicity remains not significantly different from zero. When looking at the normalised energy difference we see a plot that largely follows the theme we have seen so far. The change to

the initial Alfvén ratio produced an initial peak corresponding to the large difference in energy we began with. As the two energy levels converged, this means the value for σ_D reduced to zero with it, and we see this with the plot for σ_D being almost identical for the two cases beyond $t \approx 1$.

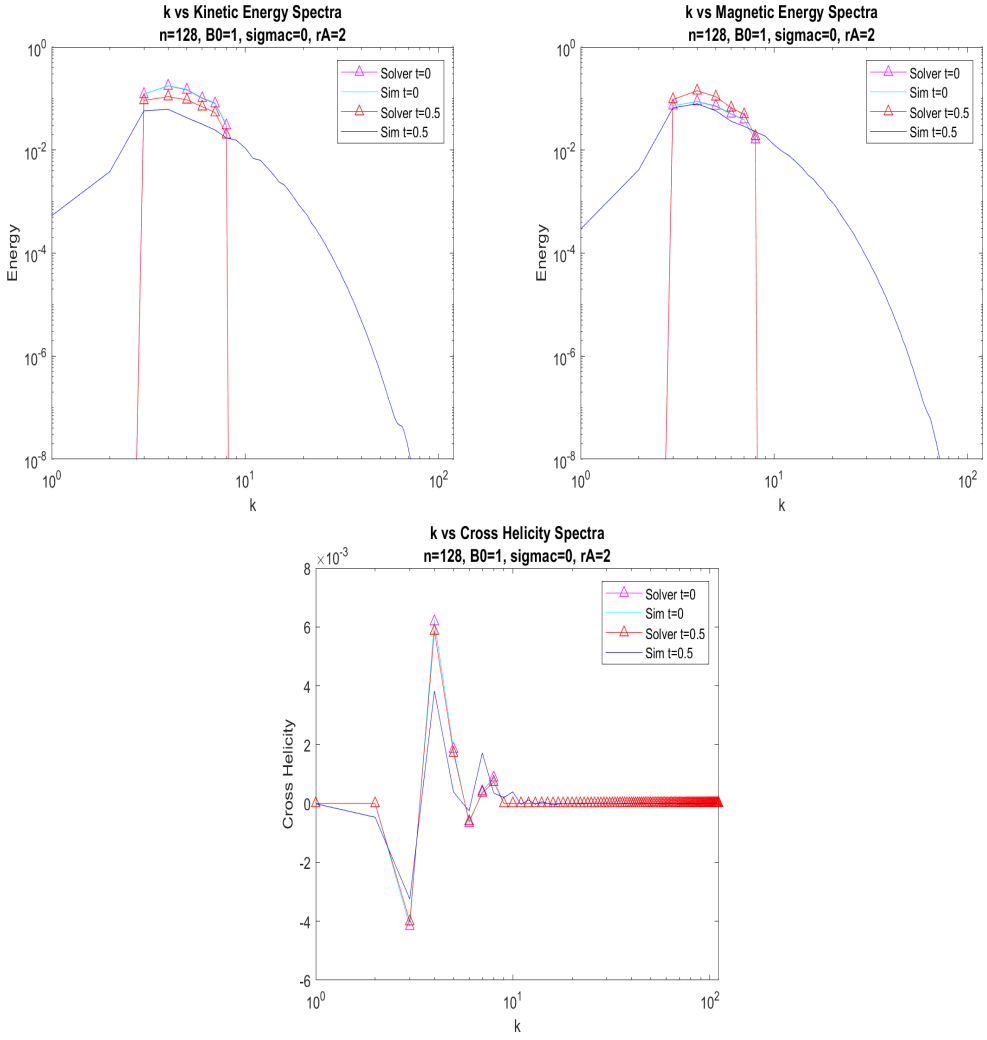

Figure 3.8: Spectra plots for the various energy measures in the run of $n = 128$, $b_0 = 1.0$, $\sigma_c = 0.0$, $r_A = 2.0$, where the solver takes its initial reference as t=0. The evolution at t=0.5 is also plotted

With regards to the spectral plots, we see total agreement in the initial spectra for both the kinetic and magnetic spectra. Notably this agreement is of the energy being confined once again to entirely within the initial wavenumber band of $3 < k < 8$. As time evolves to $t = 0.5$ the lack of turbulence leads the energy to still being contained within the same band for the MATLAB solver

results in both the magnetic an kinetic spectra. In the case of the kinetic spectra these levels have decreased a small amount from the initial conditions as the energy in the system dissipates through viscosity. Unlike this, the levels of the magnetic spectra have actually increased. As we recall there was an initial increase in the magnetic energy which peaked at around $t \approx 0.5$, and with no non-linear action to transfer the energy to the smaller scales, this leads to an overall increase in the energy spectra as well for the $t = 0.5$ plot, as the energy has not been able to transfer to the more dissipative smaller length scales. By contrast, the energy spectra plots for the simulation have evolved to a very similar plot to the corresponding $r_A = 1.0$ plots. Given that the total energies at this time were almost the same at this point, the similar shape of the spectra is not unexpected. We do still see the effect of the initial increase in magnetic energy however. The increase appears to have been balanced out by the transfer of energy between length scales, and so we see almost no change in the magnetic energy spectra between $t = 0$ and $t = 0.5$ in the initial band. The cross helicity spectra remains unchanged in shape with the updated initial Alfvén ratio, with the differences coming in the size of the peaks. In the results of the MATLAB solver, the increased initial Alfvén ratio leads to smaller spikes for the entire wavenumber range, with the biggest reduction being the values of H_c associated with wavenumbers $k = 3$ and $k = 4$. There is almost no change between the initial results and the $t = 0.5$ results, as the small decrease in kinetic energy is compensated by the peak in magnetic energy at this time. The more interesting results are in the simulation plot, where the spikes reduce greatly for smaller k, but in fact increase for $k > 6$, although large k values still present almost zero cross helicity.

Using the same conditions, but allowing the simulation to run until $t = 0.5$ before beginning the MATLAB solver we see from figure 3.9 that the initial effects of the change to the r_A have worn off. By this time the simulation values have reached the same values as they had during the $r_A = 1.0$ initial conditions for all of the quantities considered in the time plots. The result

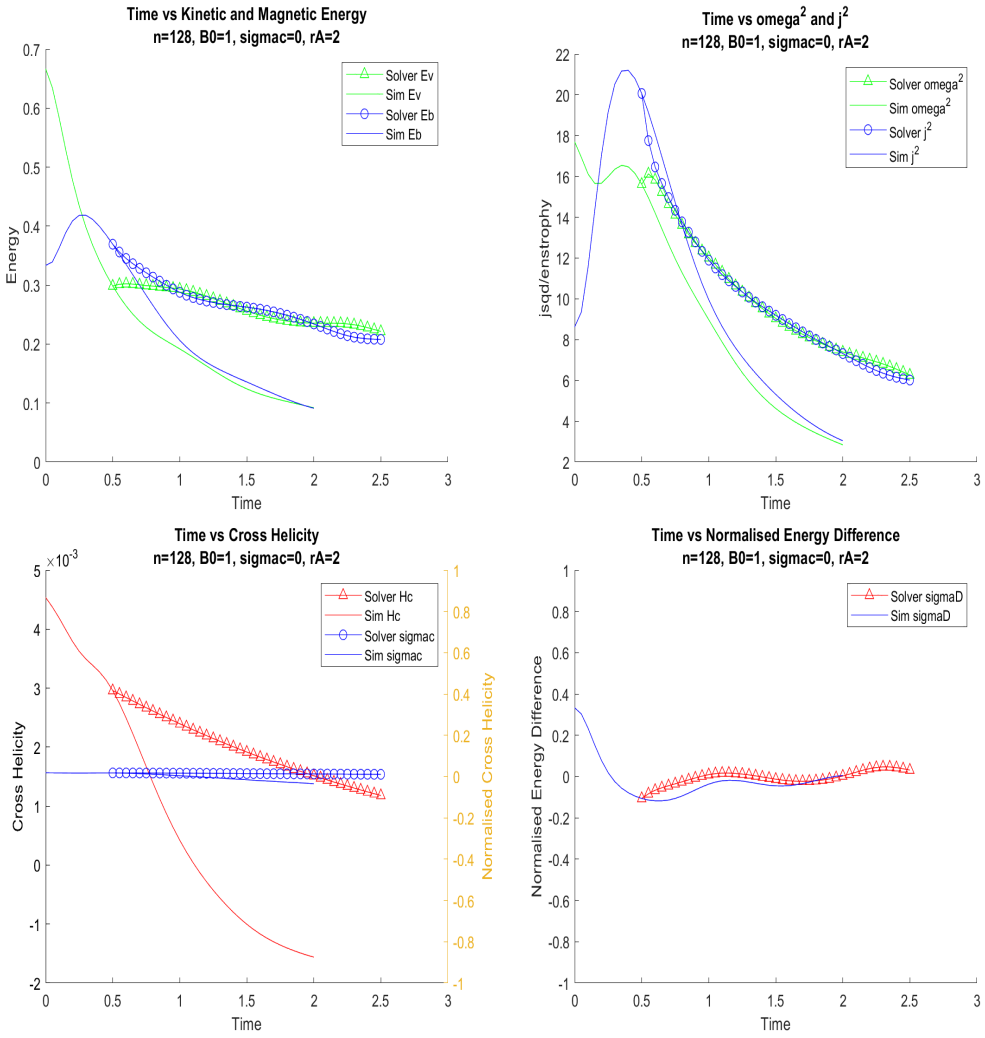

Figure 3.9: Time plots for the various energy measures in the run of $n = 128$, $b_0 = 1.0$, $\sigma_c = 0.0$, $r_A = 2.0$ beginning from t=0.5

of this is that the 'initial' conditions for the MATLAB solver when beginning from $t = 0.5$ are the same for both initial Alfvén ratios.

When we look at how the spectra plots evolve over time it is a very similar story. After t=0.5 the two systems ($r_A = 1.0$ and $r_A = 2.0$) have become almost identical, and the contribution of different wavenumber bands to the total energy is therefore also almost identical. In particular for the MATLAB solver there is no change at all in the way the kinetic and magnetic energy spectra evolve from t=0.5 to t=1, when compared to the evolution of the initial $r_A = 1.0$. The simulation evolution reads similarly to that of the MATLAB solver, though there is a small difference in both kinetic and magnetic spectra

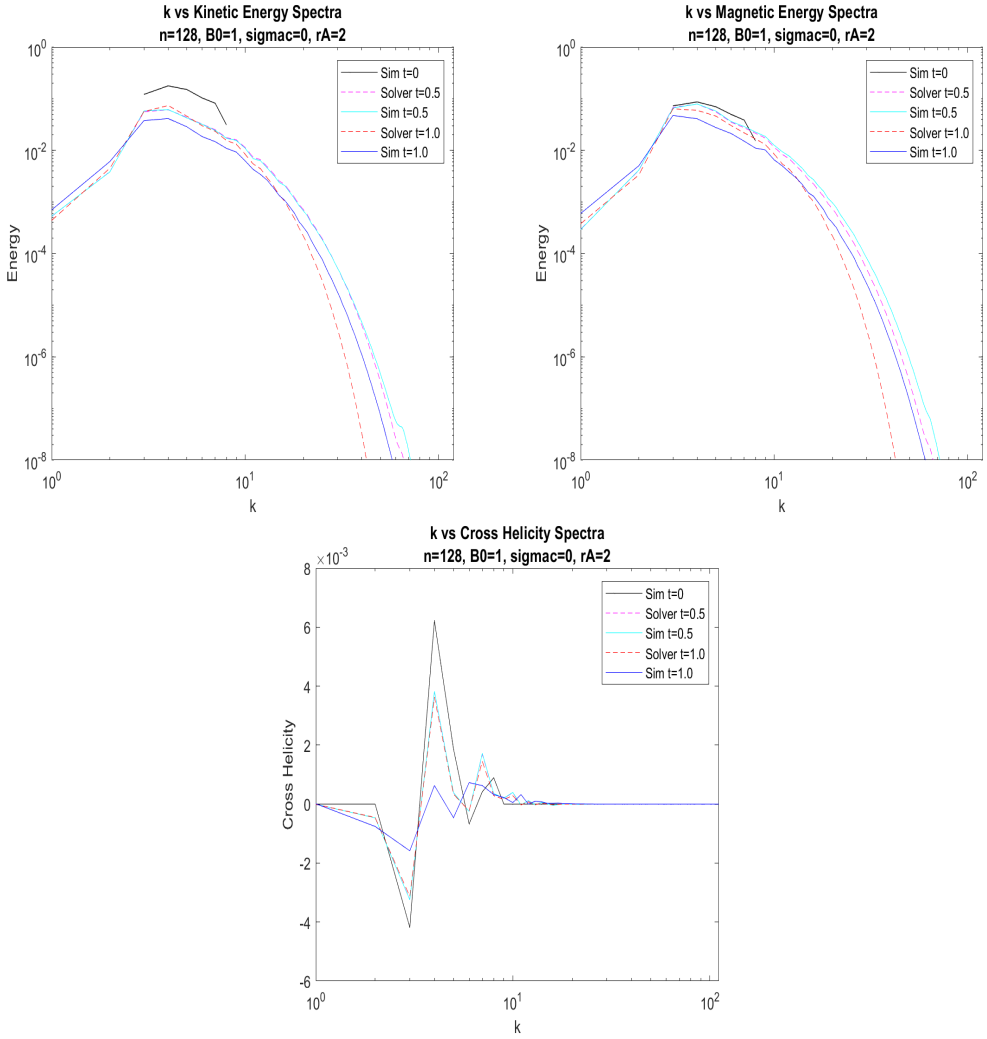

Figure 3.10: Spectra plots for the various energy measures in the run of $n = 128$, $b_0 = 1.0$, $\sigma_c = 0.0$, $r_A = 2.0$, where the solver takes its initial reference as t=0.5. The simulation values at t=0 are also plotted

at t=1. Just as in the initial $r_A = 1.0$ conditions, the simulation spectra is more spread out than the MATLAB solver values, owing to the continued replenishing of the higher wavenumber bands from the energy transfer from the lower bands. The only difference to the behaviour of the $r_A = 1.0$ initial condition is a small increase in the steepness in the dissipation range, indicating the energy has been lost slightly faster. The difference is small though, and is not noticeable in the energy plots over time, so the energy is likely not being lost at any significantly increased rate. Where we do see a noticeable difference between the two initial Alfvén ratio conditions is in the cross helicity

spectra plot. Between $k = 3$ and $k = 7$ values are consistently less for the $r_A = 2.0$ plot than the corresponding $r_A = 1.0$ plots at t=0.5, and outside that range, values are consistently more. Conversely, at t=1 the cross helicity contribution is larger for almost all values of k. The two main exceptions are the bands where $k = 3$ and $k = 4$. For $k = 3$ the cross helicity contribution is significantly less in the $r_A = 2.0$ system, and where $k = 4$ the magnitude is roughly the same, though its sign has reversed. This hints at greater transfer of energy to the smaller scales from the system with the higher initial Alfvén ratio. It was also noted previously that while the shape for the cross helicity largely remains the same between t=0 and t=0.5, the magnitude of the peaks changed significantly. This trend continues as time evolves out to t=1 with overall levels being lower for the simulation values. Values for the MATLAB solver do not change between t=0.5 and t=1 as they can no longer continue to transfer energy to more dissipative scales and they remain at larger scales where dissipation effects are still small.

Figure 3.11 shows the time plots where the initial Alfvén ratio is $r_A = 0.5$. The energy levels of the MATLAB solver before t=0.5 are almost completely reversed from the initial $r_A = 2.0$, which is simply a direct result of the calculation of the Alfvén ratio $r_A = \frac{E_v}{E_b}$ and the selection of the two initial values as reciprocals. Just as in the case of initial $r_A = 2.0$, beyond $t \approx 0.5$ the energy values – both kinetic and magnetic – are approximately equal to the initial $r_A = 1.0$ case. The biggest difference in energy based on adjusting the initial Alfvén ratio comes in the simulation values. Whereas the MATLAB solution simply flips values between $r_A = 0.5$ and $r_A = 2.0$, the simulation has a distinct difference in the peak value of the lower of the two energies. We saw in figure 3.7 that the peak magnetic energy for the simulation was $E_b \approx 0.42$, and figure 3.11 shows that the peak kinetic energy is significantly less at $E_v \approx 0.36$. This difference is accompanied by a much slower initial decrease in magnetic energy for the $r_A = 0.5$ case than there was for kinetic energy in the $r_A = 2.0$ case. Overall however, we can see now that the changes to the initial Alfvén

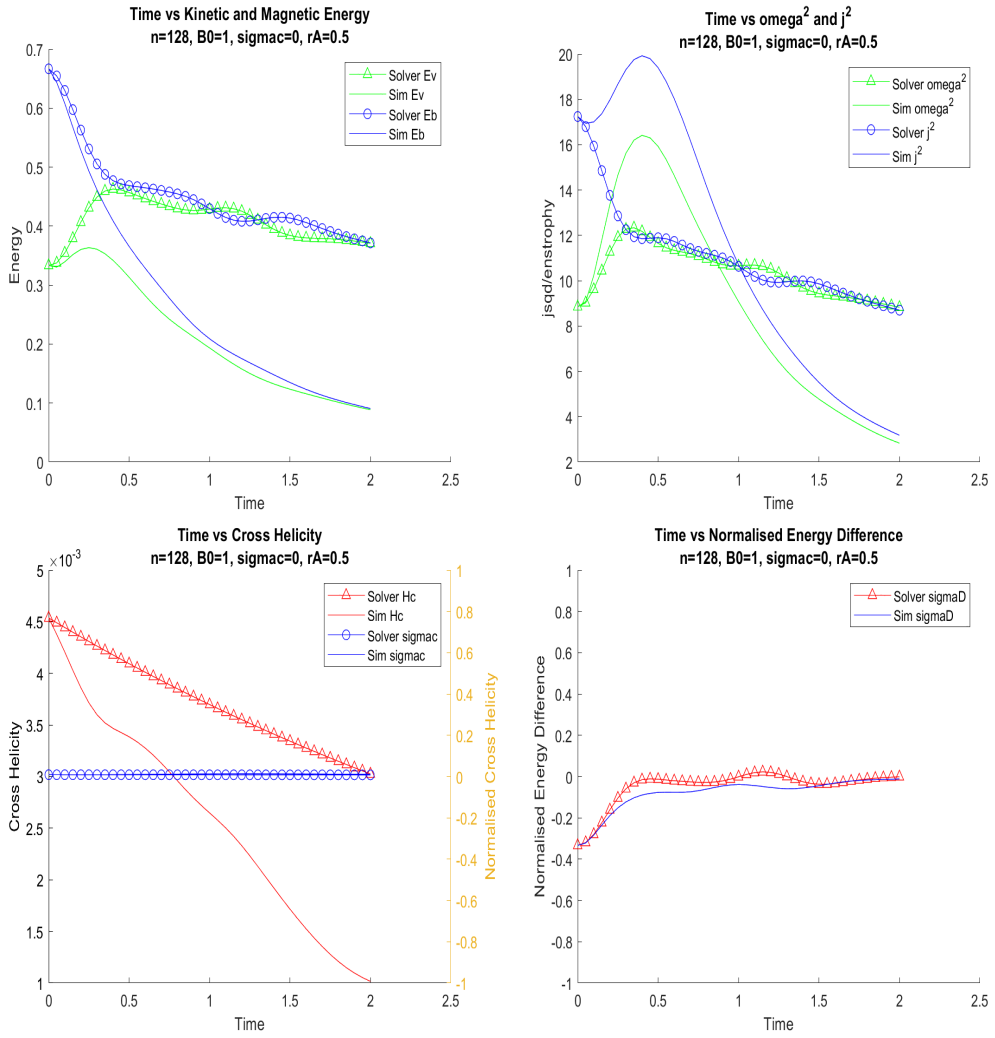

Figure 3.11: Time plots for the various energy measures in the run of $n = 128$, $b_0 = 1.0$, $\sigma_c = 0.0$, $r_A = 0.5$ beginning from t=0

ratio only have a small effect on energy levels beyond t=0.5. The effects of changing the initial Alfvén ratio on enstrophy therefore are also restricted to that initial moment. Across all three initial states we see ω^2 and j^s peaking at $t \approx 0.4$ before rapidly decreasing to nearly the same value for the simulation, or converging to the same pattern of oscillations with the same central line for the MATLAB solver. Of the three initial Alfvén ratios tested, $r_A = 0.5$ lead to the smallest peak in simulation values for ω^2, peaking at $\omega^2 \approx 20$, rather than $\omega^2 \approx 21$ in the other two cases.

Normalised cross helicity remains negligible for both MATLAB solver and simulation values, and while this is the case with the smallest reduction in non-

normalised cross helicity, it is worth remembering that the values are plotted on a scale small enough that the differences are not significant. This theme of the $r_A = 0.5$ case as a simple reflection in the early stages of the $r_A = 2.0$ case continues with the normalised energy difference as well. Where the $r_A = 2.0$ case had σ_D quickly decreasing to equilibrium, the only significant difference is here it quickly rises to equilibrium from a negative initial value. For times later than $t \approx 0.6$, there is no significant difference across the three starting states.

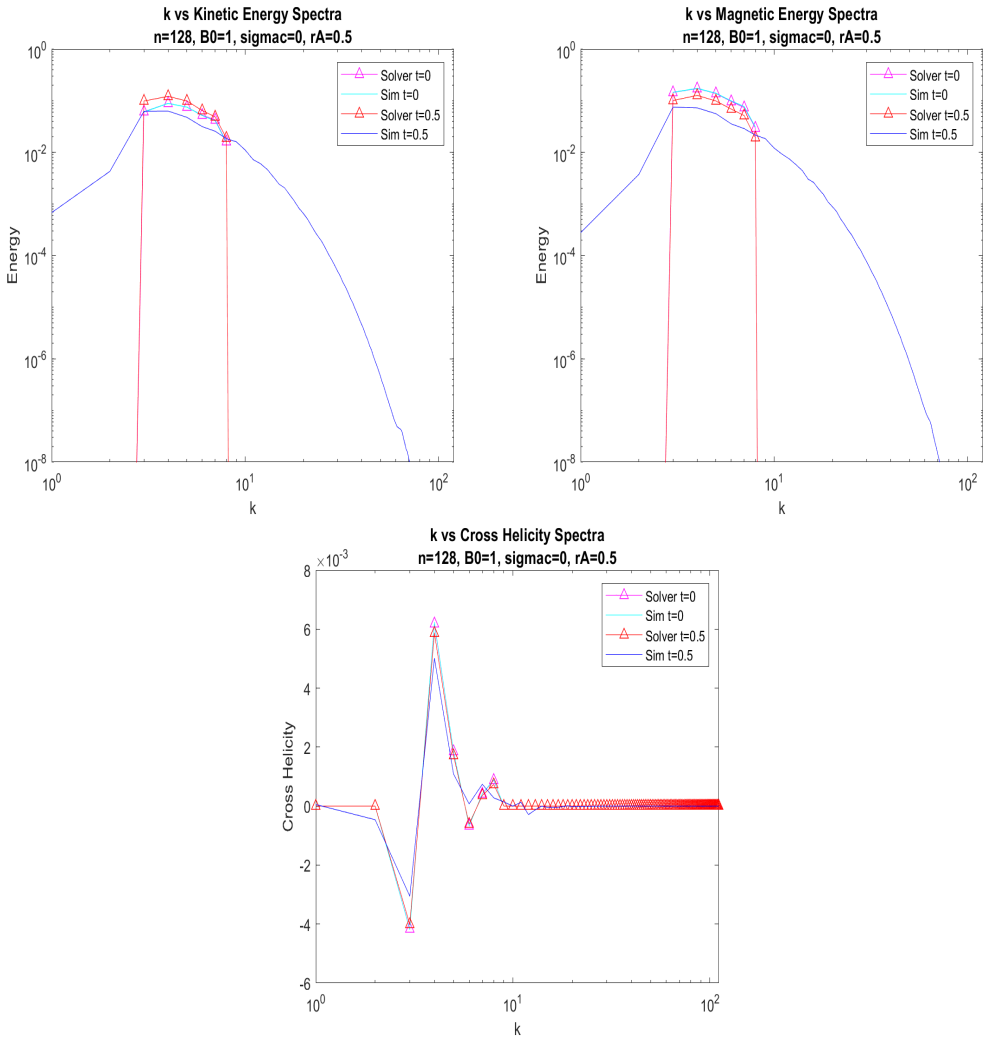

Figure 3.12: Spectra plots for the various energy measures in the run of $n = 128$, $b_0 = 1.0$, $\sigma_c = 0.0$, $r_A = 0.5$, where the solver takes its initial reference as t=0. The evolution at t=0.5 is also plotted

As we might now expect, the spectra plots for $r_A = 0.5$ (figure 3.12) show

a reversal of the $r_A = 2.0$ plots. Rather than seeing kinetic energy levels in the initial $3 < k < 8$ band starting high and dropping as they did in figure 3.8, we in fact see them start out lower and rise for the MATLAB solver values. Similarly, where previously we saw the magnetic energy levels start lower in the initial band and rise for the MATLAB solver values, now we see them starting higher and falling as time evolves to t=0.5. The short term effect of the initial Alfvén ratio becomes clear here as we see that for both the kinetic and magnetic energy spectra, regardless of the initial energy levels, the plots for t=0.5 are the same across all three states in both the linear and non-linear systems. This shows us that, at least for when σ_c is given an initial value of 0, any changes to the initial Alfvén ratio do not produce significant changes to energy levels further in the propagation of the solution. The spectra plot for the cross helicity only displays minor differences, with a slightly taller $k = 4$ peak value, and a similarly smaller $k = 7$ peak. The rest of the spectral range is roughly the same for $r_A = 0.5$ as it is for the other starting conditions, and the highlighted differences only become noticeable on the small (10^{-3}) scale.

The plots of the time delayed MATLAB solver provided no new insight or any different activity to what we have already seen from previous plots. Just as they had in the case of $r_A = 2.0$, by the time the turbulence was 'turned off' for the MATLAB solver, values had returned to the same level as in the initial $r_A = 1.0$ case, so there was no significant difference in the long term evolution of either the turbulent or non-turbulent systems across the different initial Alfvén ratios.

Apart from the initial conditions we also see no significant change to the kinetic or magnetic energy spectra plots. The cross helicity spectra does show a few differences however. Where previous plots have shown H_c to have mostly high spikes at a few wavenumber bands, these spikes tend to be smallest for the $r_A = 0.5$ case. At t=0 the differences between all three systems is negligible, and at t=0.5 there is less spread to the smaller length scales by the $r_A = 0.5$ case than either of the other two, though the overall shape of the graphs are

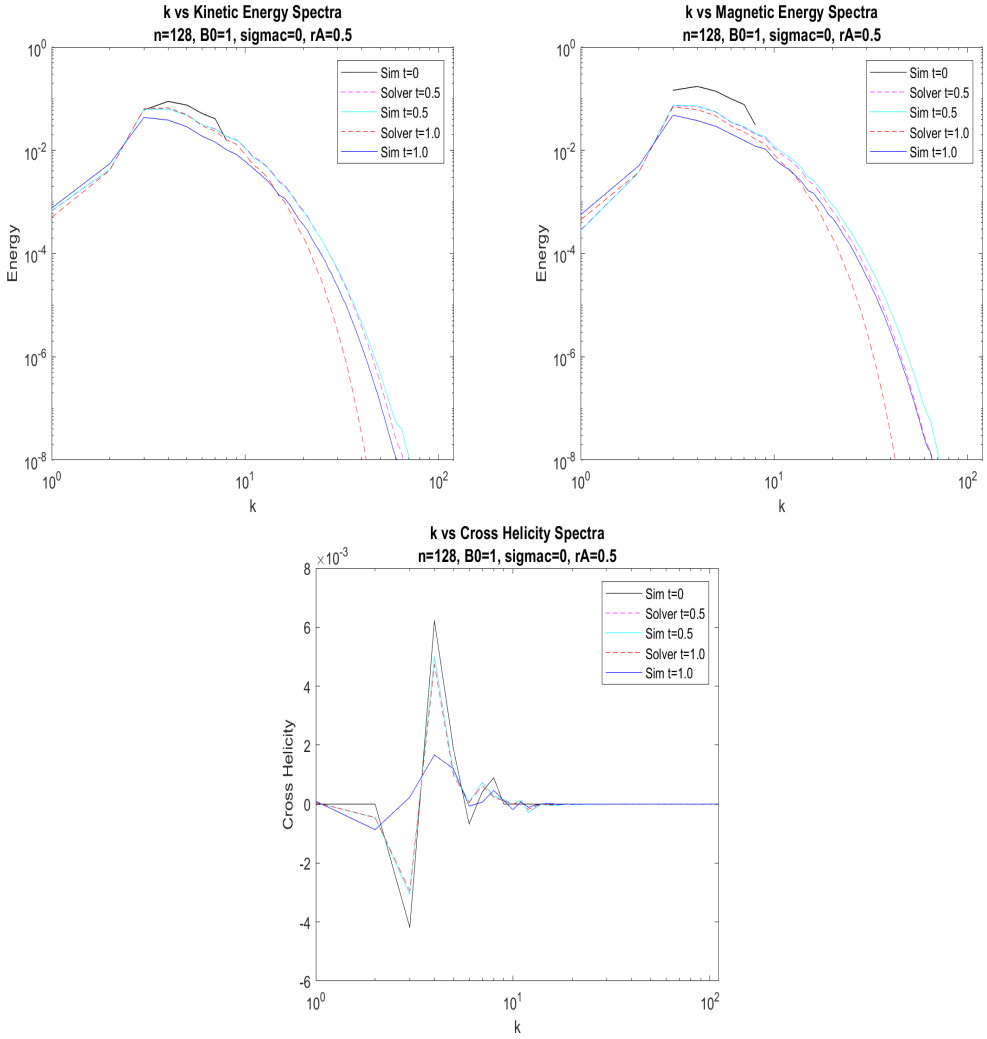

Figure 3.13: Spectra plots for the various energy measures in the run of $n = 128$, $b_0 = 1.0$, $\sigma_c = 0.0$, $r_A = 0.5$, where the solver takes its initial reference as t=0.5. The simulation values at t=0 are also plotted

still mostly the same. The only significant differences come when the solutions have been allowed to evolve through to t=1. In each case the plots do not change at all from t=0.5 for the MATLAB solver solutions, but the simulation solutions are noticeably different. The $r_A = 0.5$ initial condition shows the least amount of spread for cross helicity, with significantly higher values within the $3 < k < 8$ range and mostly nothing beyond.

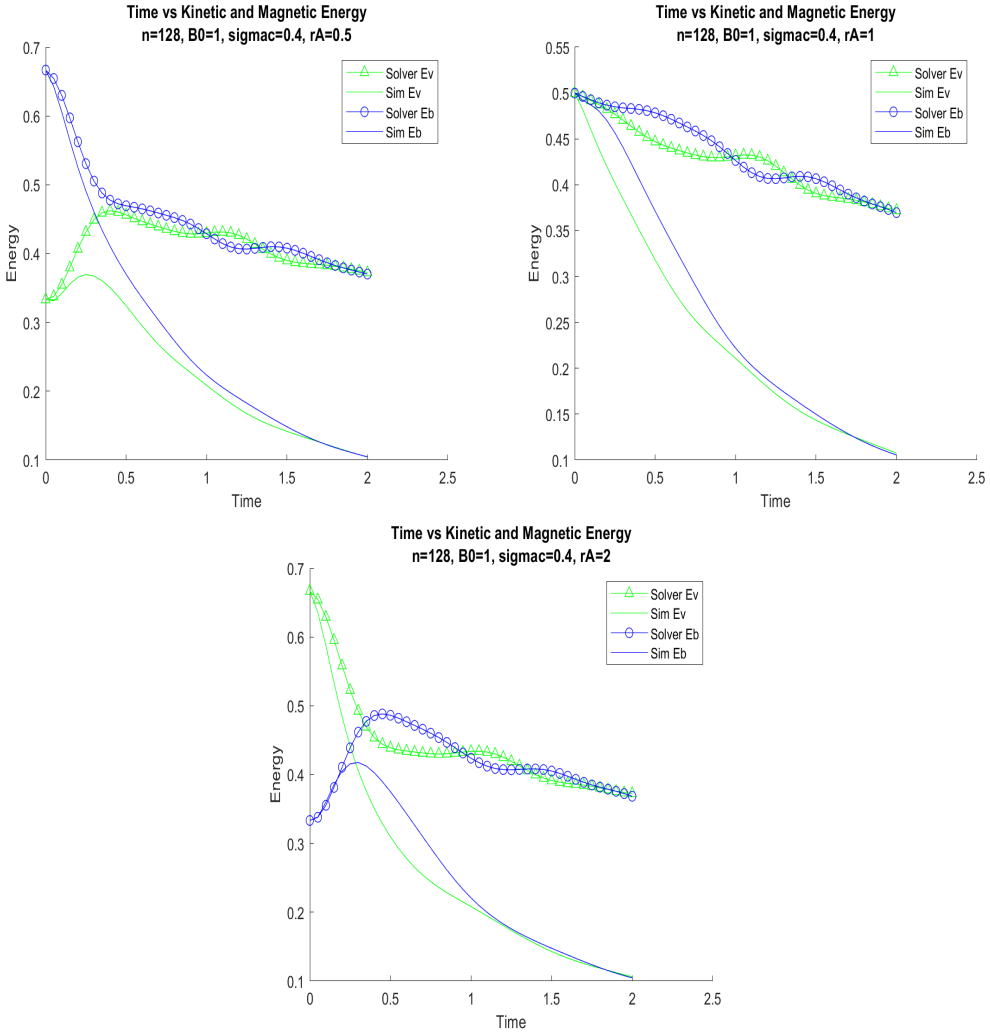

Figure 3.14: Energy plots for various initial Alfvén ratios when $b_0 = 1$ and initial $\sigma_c = 0.4$

We saw through the plots of initial $\sigma_c = 0$ that changes to the initial Alfvén ratios did not lead to long lasting changes to the energy of the system, and figure 3.14 shows that the same holds for an initial value of $\sigma_c = 0.4$. We see that for all three plots, despite how they began, the energies were the same once the solutions were able to evolve past t=0.5. When we look at the plots where the initial Alfvén ratio was $r_A = 2.0$ or $r_A = 0.5$ we see defined peaks in the simulation solutions for the value of whichever energy began lower at around $t \approx 0.4$, and it is beyond this point where energy levels converge between the three systems. This peak notably only exists in the simulation solutions. For the MATLAB solver solutions, energy values converge to the

central line marked out by the oscillations for later times.

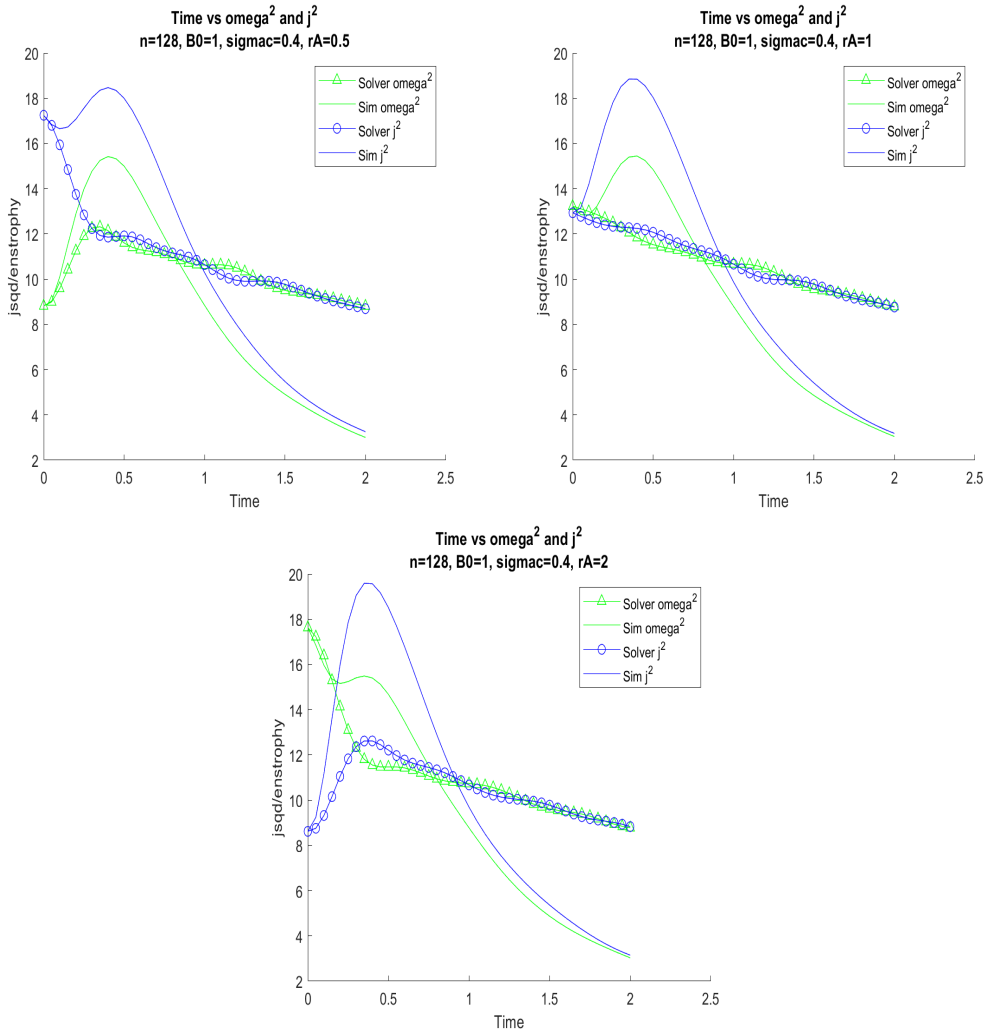

Figure 3.15: ω^2 and j^2 plots for the various initial Alfvén ratios, where $b_0 = 1$ and $\sigma_c = 0.4$

The enstrophy plots in figure 3.15 show much the same story as the energy plots. Regardless of the initial conditions, both ω^2 and j^2 quickly attain the same shape. In the case of the MATLAB solver solutions this shape is an oscillating pattern with a linearly decreasing central line. For the simulation solutions, this is a peak in both quantities before a much steeper decrease. These peaks in the simulation solutions are key to the presence of the initial energy spikes in figure 3.14. Localised eddies build up in the turbulent systems before transferring the energy to smaller scale eddies which allows the energy to dissipate much faster than in the linear MATLAB solver solutions, which

are dependant only on the viscosity to dissipate energy.

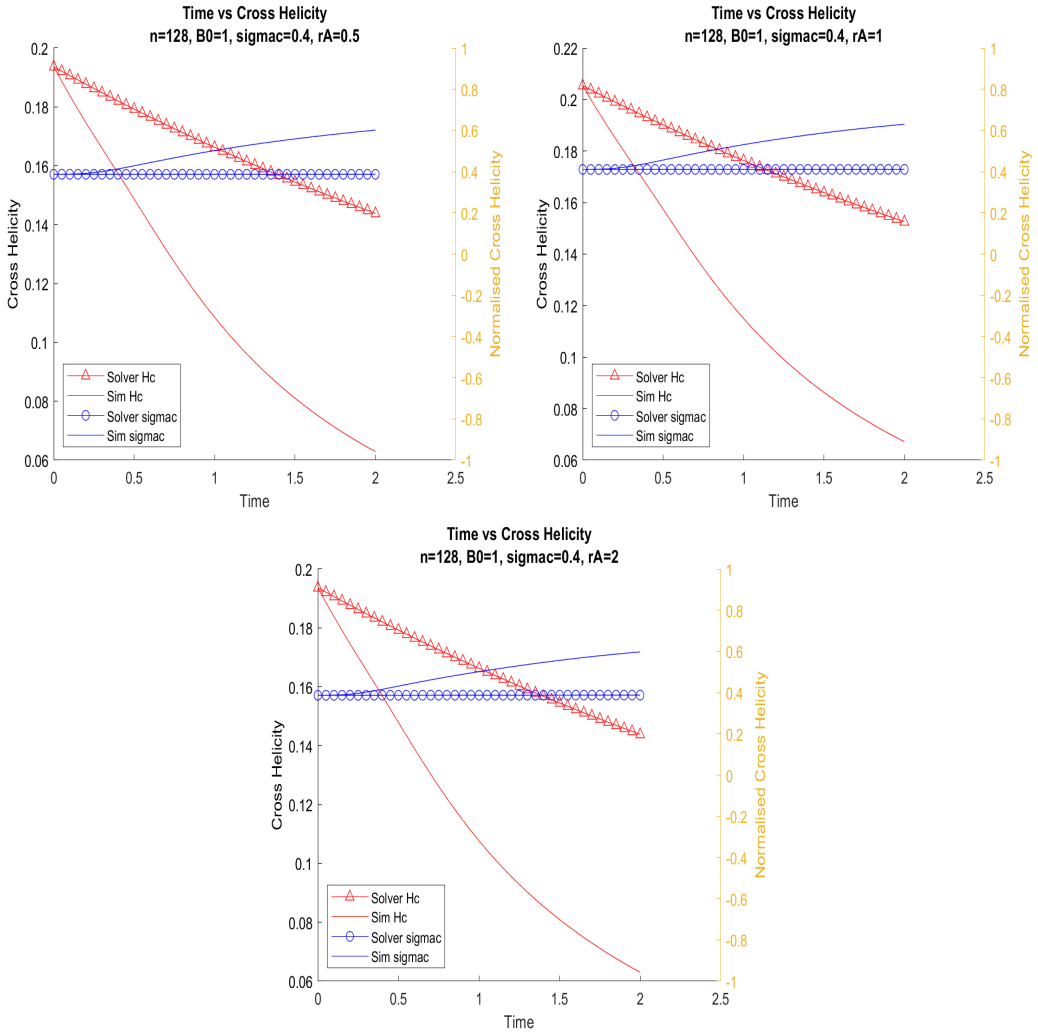

Figure 3.16: Plots for the cross helicity and its normalisation over time for various initial Alfvén ratios, where $b_0 = 1$ and $\sigma_c = 0.4$

Figure 3.16 shows the first time we see cross helicities on a significant scale. The three systems all show the same behaviour, indeed the plots for initial $r_A = 2.0$ and $r_A = 0.5$ are almost identical. Specific values for initial $r_A = 1.0$ are larger than in the other two cases, but the overall shape remains the same. There is a consistent linear decrease in the MATLAB solver values, but as the turbulent systems are able to more efficiently dissipate the energy, the cross helicity for the simulation solutions decreases much faster. In the normalised quantities, we see that the lack of non-linear activity means that for the MATLAB solver solutions the decrease in energies contributes equivalently

to both the cross helicity and the energy total used to normalise it. This causes the normalised cross helicity to remain at its initial value of 0.4 for the entire run. On the other hand, we see that for the simulation, the normalised cross helicity increases steadily, which shows that the total energy decreases faster than H_c.

No real differences showed up in the plots for the normalised energy difference compared to the runs with initial $\sigma_c = 0$. Just as in that case, the changes to the initial Alfvén ratio affected the initial values, but they stabilised before t=0.5. In fact, this is common for all of the initial conditions I tested under the magnetic field $b_0 = 1$. Regardless of the initial value for either r_A or σ_c, the normalised energy difference always returns to hover near to zero for both the linear and turbulent systems. Refer to appendix B to see the plots of this. Fluctuations around zero do decrease as the initial σ_c increases, but for the most part σ_D remains consistent across the different initial conditions.

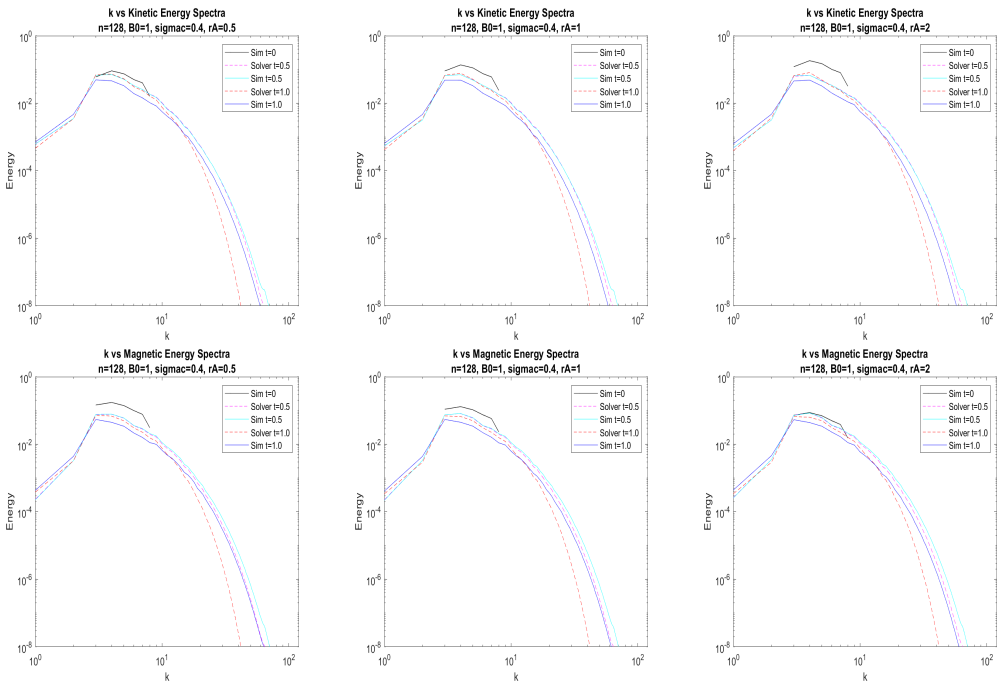

Figure 3.17: Energy spectra plots for the various initial Alfvén ratios with $b_0 = 1.0$ and initial $\sigma_c = 0.4$. The solver takes its initial reference as t=0.5. The simulation values at t=0 are also plotted

The energy spectra plots in figure 3.17 show the same consistency of results as the previous time based plots. For the greatest potential difference among the different initial conditions, the plots used are the ones where the MATLAB solver was initialised using the simulation data at t=0.5, since this was the period that showed the greatest change when the normalised cross helicity was initially zero. As has come to be expected, the only significant difference across different Alfvén ratios were the plots for the initial spectra, when the different initial conditions still have an effect. By the time we reach t=0.5 the differences in initial conditions have lost their influence, so the plots all show the same shape and values.

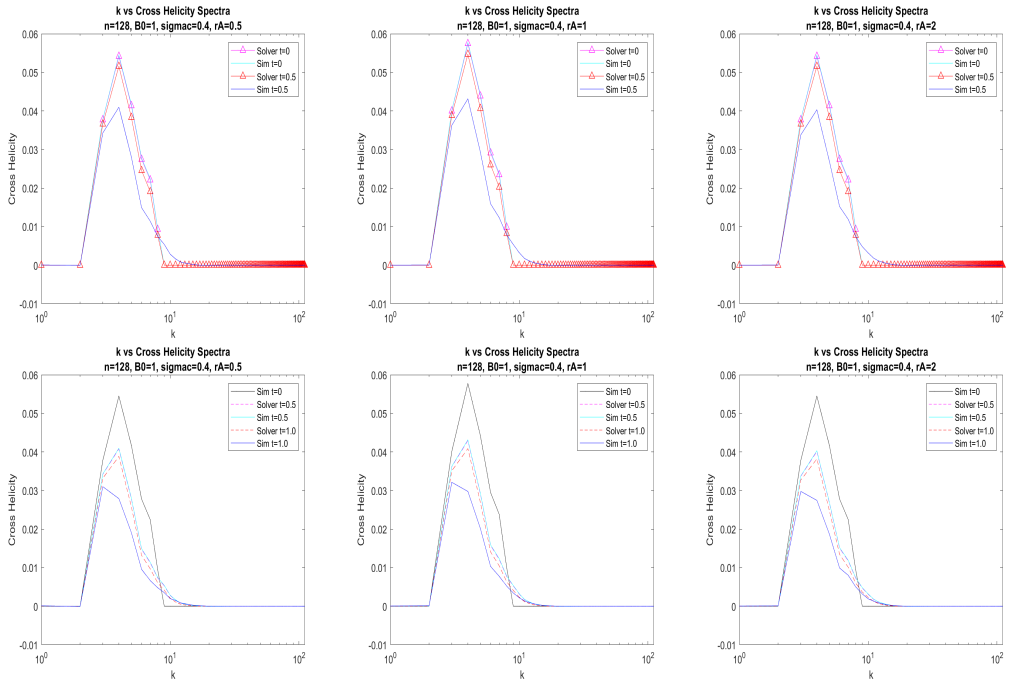

Figure 3.18: Cross helicity spectra plots for the various initial Alfvén ratios with $b_0 = 1.0$ and initial $\sigma_c = 0.4$. Values are plotted for the MATLAB solver being initialised with both t=0 and t=0.5 simulation values

We see the same happening in the plots for the cross helicity spectra in figure 3.18. This time values are plotted for the MATLAB solver being initialised with the values for both t=0 and t=0.5 and in both cases the effect is the same. We see slightly higher values for the plots that come from an initial Alfvén ratio of 1.0, but it is small, and the other two sets of initial conditions

give the same values. As the solutions evolve this difference decreases and becomes negligible by the time the solutions have reached t=1. Differing from the individual energy spectra, the results themselves here are significantly different to the results from the runs which had initial $\sigma_c = 0$. Most notable is the values now are non-negative, and forming one single pillar, rather than several peaks both positive and negative. Values are also a factor of ten larger in general than they were when the initial value of σ_c was reduced.

We have already seen how the changes due to different initial Alfvén ratios do not last beyond $t \approx 0.5$, and this remains true when the the initial value of σ_c is increased again to 0.9. However the solutions do become significantly different as we move through different initial values of the normalised cross helicity. This difference is clearest between $\sigma_c = 0.9$ and the other two values used. We see just how this difference is expressed in figure 3.19 below.

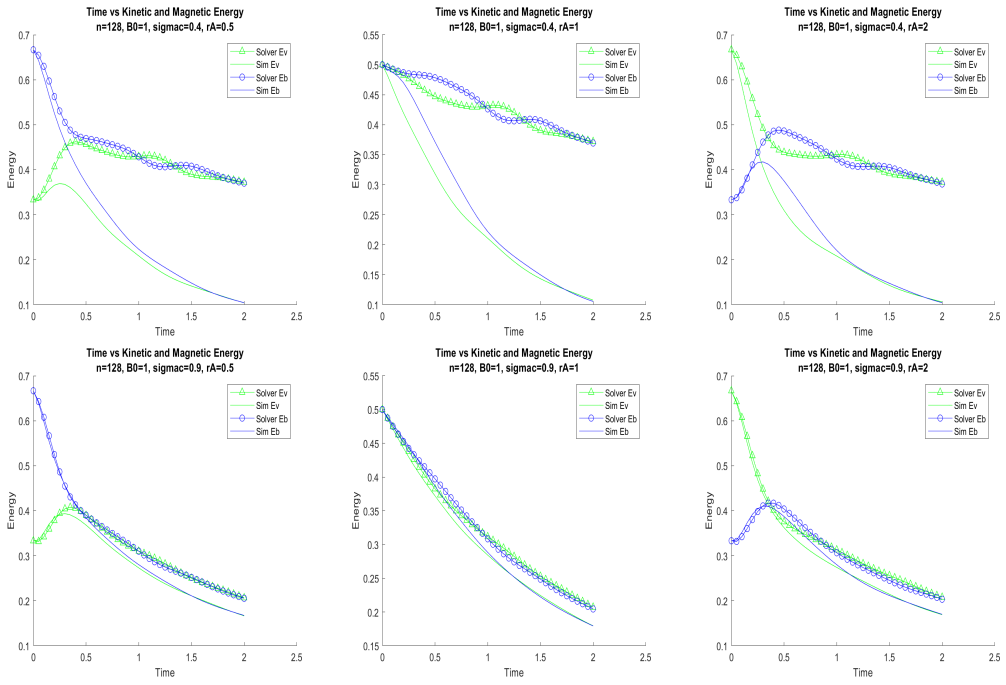

Figure 3.19: Energy plots for the various initial Alfvén ratios for σ_c values of 0.4 and 0.9

The difference is most clear in the MATLAB solver solution. With the higher σ_c value, there is a much steeper decrease in the energy levels compared to lower σ_c values. This leads it to provide a much more similar solution to

the simulation values. There is also a significant reduction in the amplitude of the oscillations of the energy levels. The simulation also provides a different solution under these initial conditions, though it is less noticeable. We see that when $\sigma_c = 0.9$ the kinetic and magnetic energies are much closer to each other in value once the solution has evolved past the typical t=0.5 time which we have noted already acts the upper limit of the time period where the effects of the initial Alfvén ratio are noticeable.

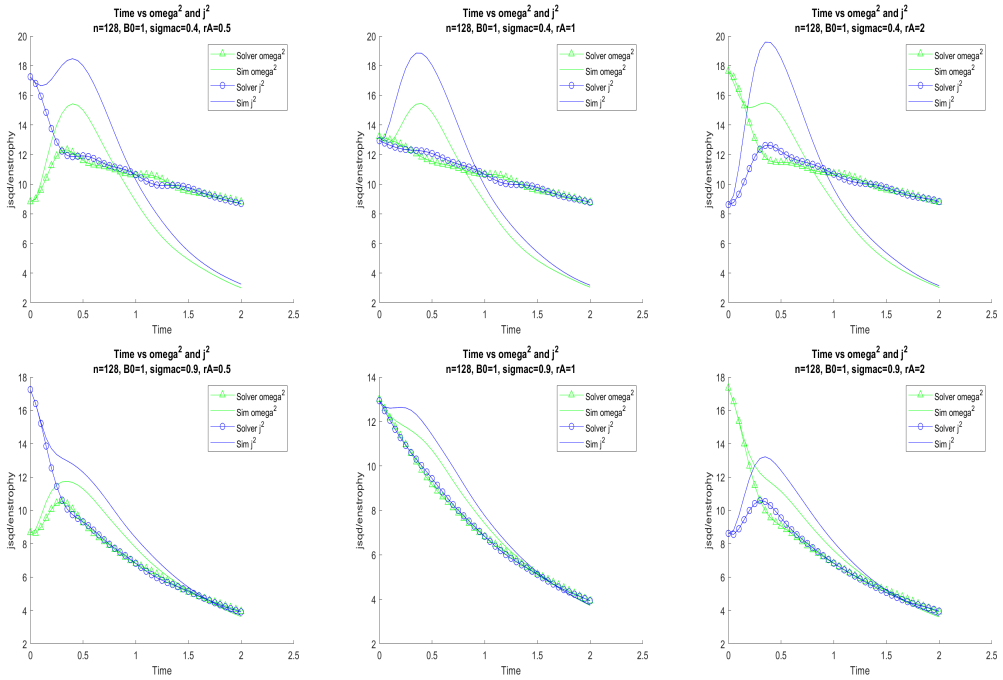

Figure 3.20: Enstrophy plots for the various initial Alfvén ratios for σ_c values of 0.4 and 0.9

Figure 3.20 shows how the difference made by increasing the initial σ_c closer to a value of 1 affects the enstrophy in much the same way. Again we note how in the case of $\sigma_c = 0.9$ the linear system is much more similar to the turbulent one than it is when $\sigma_c = 0.4$. It is also very clear that although the systems may start with the same values for all initial conditions, when σ_c has an initial value of 0.9 there is a clear trend toward smaller values for ω^2 and j^2. When σ_c had an initial value 0.4, we saw ω^2 consistently peaked in the simulation data at a value just below 16, for all three initial Alfvén ratios. When σ_c is increased to 0.9 however, this peak value for ω^2 is much lower, approximately

12. In two cases then ($r_A = 1.0$ and $r_A = 2.0$), once the solution has evolved to the time where this peak should occur, ω^2 is still higher than this value and so we do not see the peak, rather a small bump. The same occurs with j^2, which in would peak at a value between 18 and 20 when σ_c was initialised at 0.4, but would peak just below 13 with σ_c initialised at 0.9 (now with $r_A = 0.5$ and $r_A = 1.0$ being the Alfvén ratios that have the peak covered by the high initial j^2). It is also noteworthy that the peak value of j^2 is much more consistent for $\sigma_c = 0.9$. Consider as well how, just as the energy plots showed a significantly faster decrease when $\sigma_c = 0.9$ so do the ω^2 and j^2 plots.

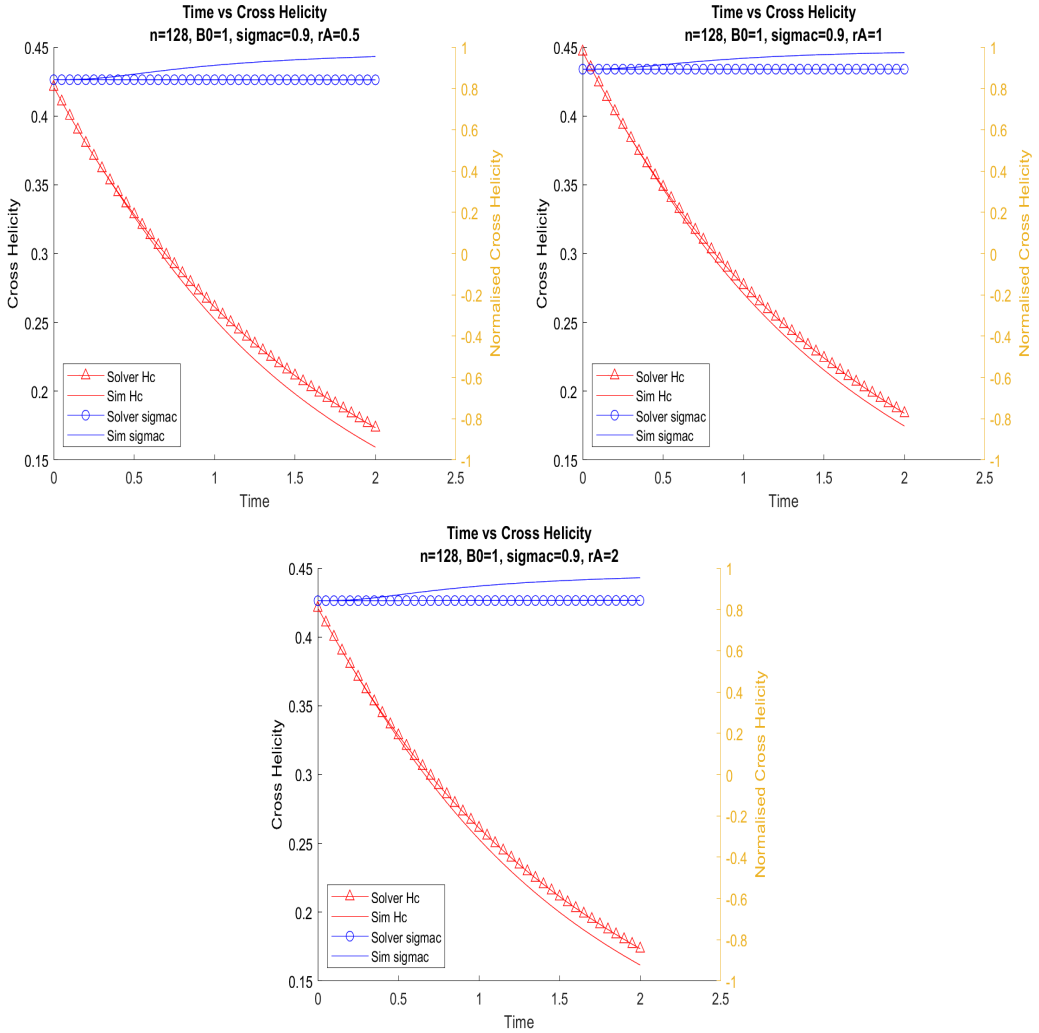

Figure 3.21: Plots of the cross helicity and its normalisation for various initial Alfvén ratios, with $b_0 = 1.0$ and initial $\sigma_c = 0.9$

The cross helicity and its normalisation are where there are the biggest

changes between the various initial σ_c values. Figure 3.21 shows the particular case where $\sigma_c = 0.9$ is the initial conditions. Refer to appendix B for a full side-by-side comparison of the effects of changing both σ_c and r_A. With the initial σ_c set to 0.9 we see the clearest change to the cross helicity is the scale. Rather than having a maximum value of $H_c \approx 0.21$, as with $\sigma_c = 0.4$, or $H_c \approx 5 \times 10^{-3}$, as with $]\sigma_c = 0.0$, the cross helicity now begins at $H_c \approx 0.45$ for the system using an initial $r_A = 1.0$. The overall shape of the simulation data remains the same as in earlier plots, though now we see the values for the MATLAB solver solution decreasing much faster than previously and keeping more similar to the the simulation values. The normalised cross helicity shows a similar story to what we saw when it was initialised at 0.4. The MATLAB solver shows the cross helicity remaining constant, showing how the total energy decreases at the same rate as the cross helicity, whereas for the simulation σ_c increases over time, showing how the total energy in the system decreases faster than the cross helicity.

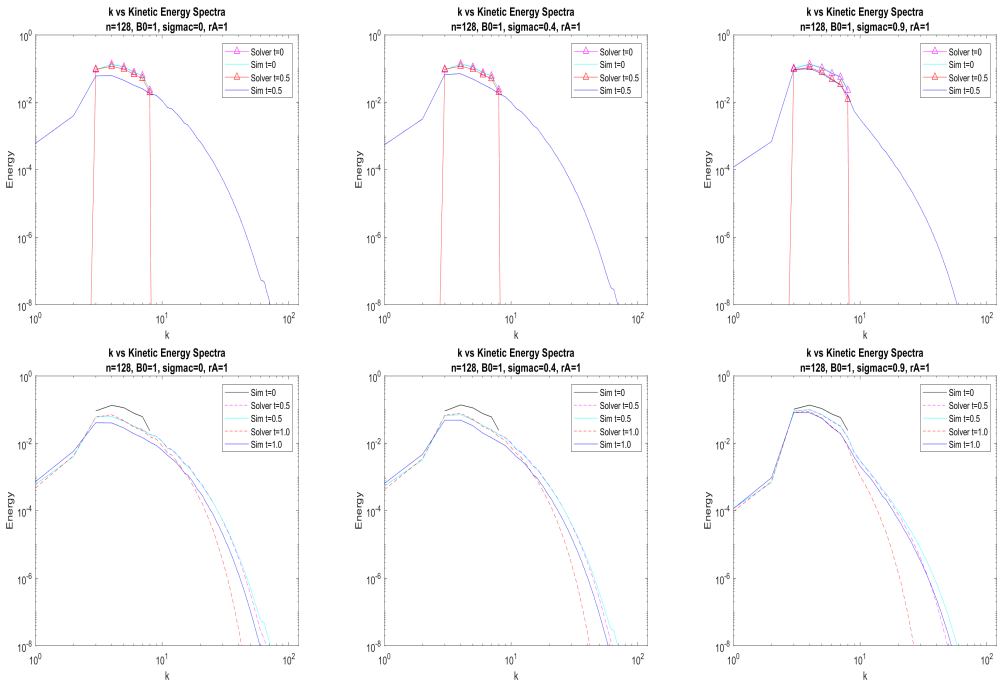

Figure 3.22: Kinetic energy spectra plots for the various values of σ_c with the MATLAB solver initialised at both t=0 and t=0.5

As with previous values for σ_c, changing the initial Alfvén ratio does not

have a significant impact on the spectra plots beyond the initial values. Figure 3.22 shows what effect the initial normalised cross helicity can have though, in particular for $\sigma_c = 0.9$ compared to 0.4 or 0.0, which themselves are very similar. Compared to the lower σ_c values, when $\sigma_c = 0.9$, there is less transfer of energy from the initial band of wavenumbers $3 < k < 8$ to the larger ks, evidenced by the steeper drop off in energy for the outer ranges, indicating that they are being replenished less by larger scales breaking down. We also see this as there is a much smaller drop in energy levels within that initial band. There is still some transfer of energy in the simulation, enough to maintain energy levels in the smaller length scales, but in the MATLAB solver where there can be no energy transfer after the no-linear activity was halted at t=0.5, there is a significantly steeper drop in energy levels. The behaviour of the magnetic spectra is the same as the kinetic spectra.

We can see in figure 3.23 that overall cross helicity values are significantly higher, around twice as much for an initial value $\sigma_c = 0.9$. Overall shape is mostly retained, with the most significant difference being how much more similarly the values for the two systems decrease as time moves on. When $\sigma_c = 0.4$ the values for the cross helicity decrease for the simulation values but significantly less for the MATLAB solver, however with the σ_c increased, the cross helicity of the two systems decreases by almost the same amount. The amount by which it decreases is also proportionally less for the higher σ_c cases, as the energy loss was also less.

We have seen that the initial Alfvén ratio of a system tends to have only a very small effect on that system beyond the initial moments, no matter whether the system supports turbulent motion or not. Additionally, we have seen that the effect of the initial value for the normalised cross helicity of the system only becomes significant as it grows near to 1, with $\sigma_c = 0.9$ the only tested value that produced a noteworthy difference across all combinations of initial conditions I tested. The biggest factor in any difference between sys-

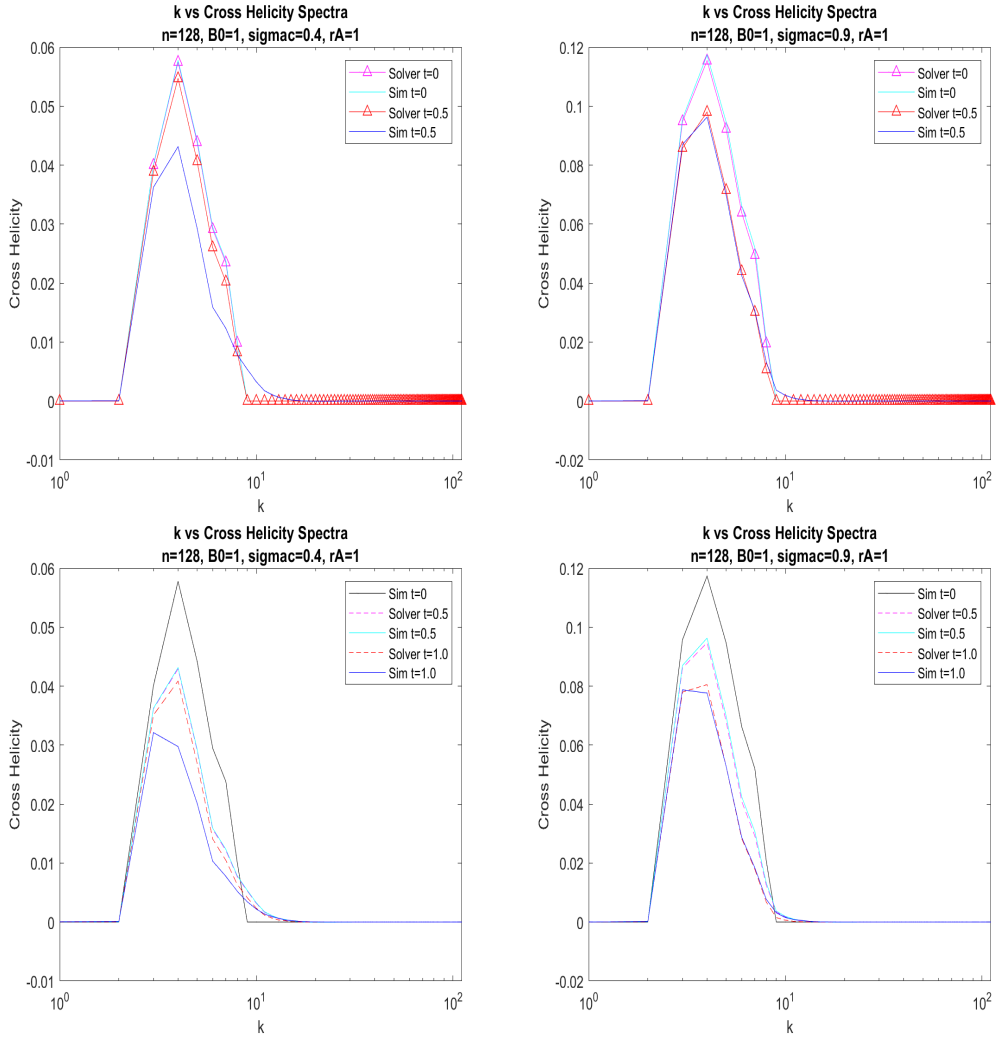

Figure 3.23: Comparison of spectra plots of the cross helicity between initial σ_c values of 0.4 and 0.9. Plots are compared where the MATLAB solver was initialised t both t=0 and t=0.5

tems was, at least when the magnetic field strength was $b_0 = 1.0$, was (as expected) the presence or absence of non-linear turbulent activity. This was particularly evident in the plots of the energy spectra, which clearly showed how when there is no transfer of energy to smaller length scales, the energy cannot dissipate as efficiently. For higher initial values of σ_c (nearer to 1), the differences between turbulent and linear systems was significantly less than for systems with lower initial values.

A Small Note on Resolution

Part of the process of obtaining the data for the plots used throughout this thesis involves performing a Discrete Fourier Transform. The discretisation in this transform has thus far mostly been presented at a resolution of $128 \times 128 \times 128$, though higher (or lower) resolutions are certainly possible. Lower resolutions were in fact used during the testing phase to obtain results faster as they require performing less calculations. Higher resolutions allow for more accuracy, and can model more energy transfer between length scales, but come at the expense of requiring more computational power. This computational requirement limited my ability to use higher resolutions, but we can see in figure 3.24 the plots produced by such a run.

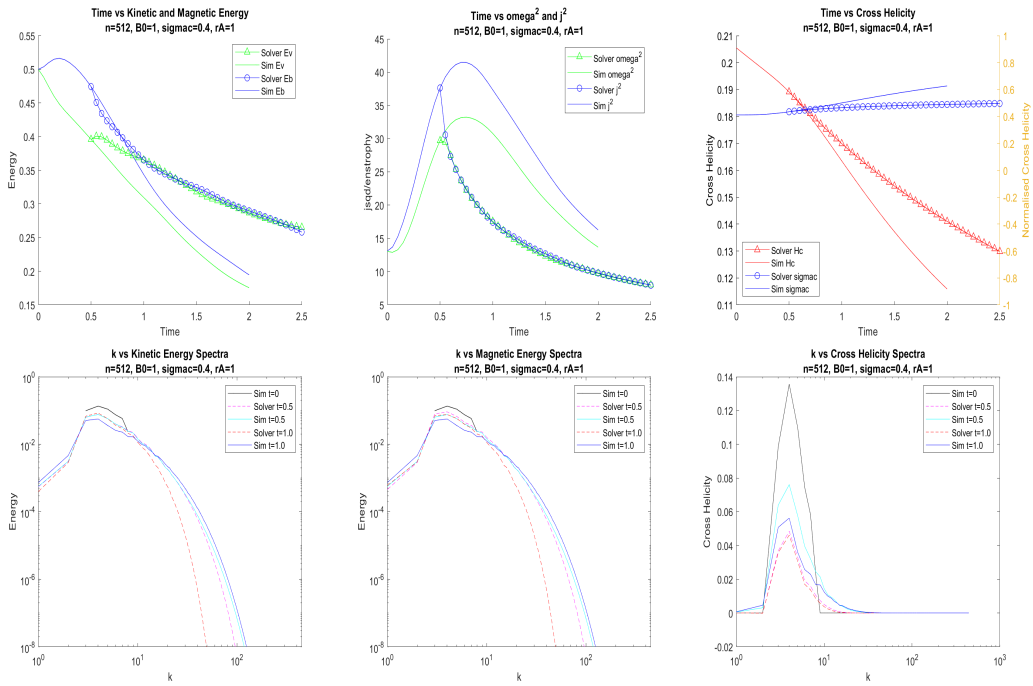

Figure 3.24: Plots from a run at a higher resolution $n = 512$, under conditions $b_0 = 1.0$, $\sigma_c = 0.4$, and $r_A = 1.0$. MATLAB solver conditions were initialised from t=0.5

The first significant difference we see from the lower resolution runs is the location of the peaks of ω^2 and j^2. Not only are the values significantly higher than in any run we saw with the lower resolution, but they occur significantly

later, at $t \approx 0.7$, with more energy able to build up before beginning to cascade. We are also able to see now that the normalised cross helicity does in fact increase over time, but with less energy transfer at lower resolutions this effect is not as noticeable. In the spectra we see energy and cross helicity much more spread out over a wider range of wavenumber bands, as we have allowed more interaction between length scales.

Magnetic Field Strength $b_0 = 2.0$

Since the strength of the magnetic field directly affects the behaviour of the fields in MHD, we might expect to see differences in the plots by adjusting the uniform magnetic field strength to $b_0 = 2.0$. Based on the lack of impact changing r_A had, I have chosen to focus only on a value of $r_A = 1.0$ for this section.

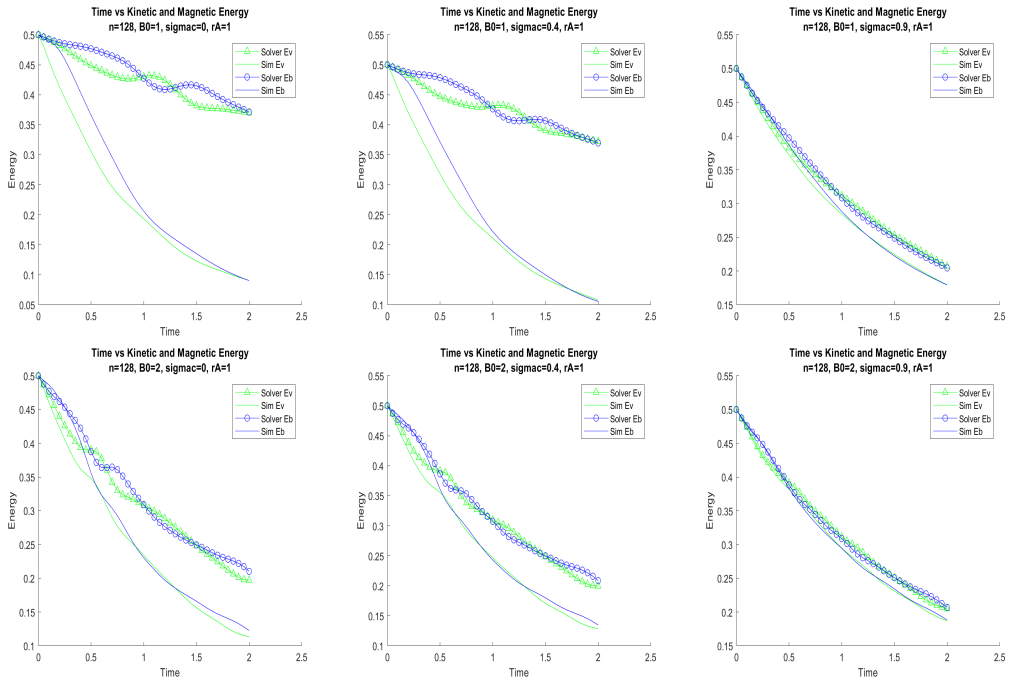

Figure 3.25: Energy plots for various initial values of σ_c, comparing $b_0 = 1.0$ with $b_0 = 2.0$

Figure 3.25 shows the comparison between energy levels when the magnetic field strength is increased. The greater magnetic field leads to an increased

frequency in the observed oscillations, producing a less smooth curve, particularly in the simulation values. Increasing the initial value of σ_c reduces this effect, with both the MATLAB solver and simulation showing smoother curves and more similar energy values when σ_c is higher. The MATLAB solver is affected significantly more than the simulation by the increase to the magnetic field strength, most notably in the two lower σ_c initial conditions. Energy dissipates much more quickly from the linear system when b_0 is higher. Since the linear system can only depend on the magnetic field strength and inefficient dissipation at large length scales, it is not unexpected that it would have a larger effect than on the simulation, which experiences most of its reduction in energy through turbulent activity transferring energy to the smaller scales where dissipation is more efficient. The change in b_0 does affect the turbulent system, though not as strongly. Interestingly, when the initial conditions set $\sigma_c = 0.4$ the final energy in the simulation was higher.

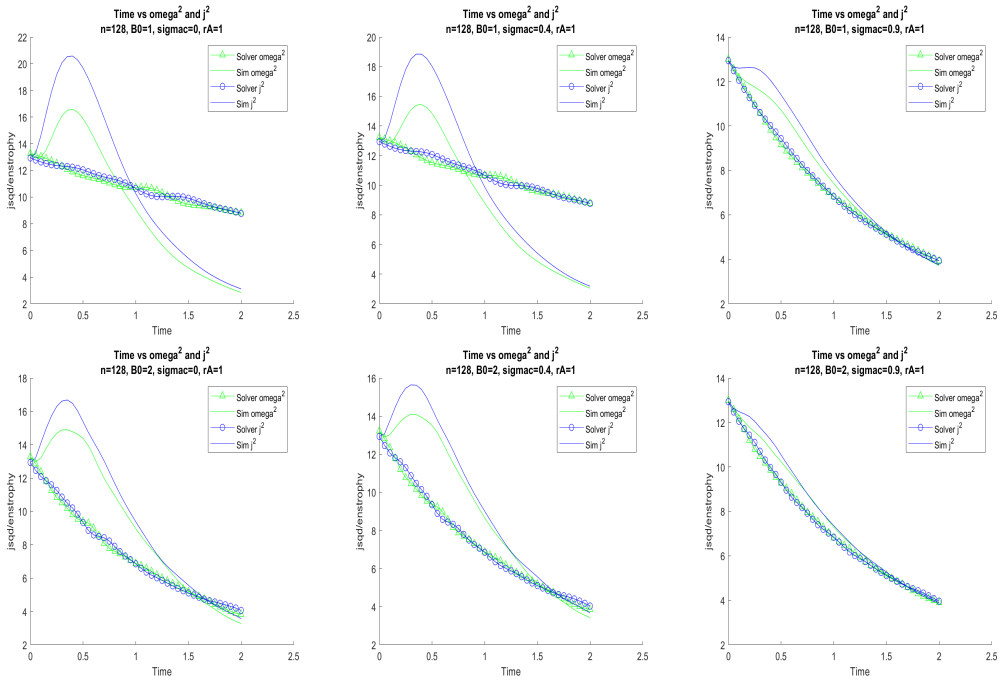

Figure 3.26: Enstrophy plots for various initial values of σ_c, comparing $b_0 = 1.0$ with $b_0 = 2.0$

In figure 3.26 we see the corresponding plots of ω^2 and j^2 to the energy plots in figure 3.25. As we saw with the energy previously, the smallest effect seen

by reducing b_0 is in the systems with $\sigma_c = 0.9$. In the simulation runs, we see no change to the behaviour of ω_c and j^2, though the values are consistently less than the corresponding runs from the weaker magnetic field. In the MATLAB solver solutions, we notice a significantly faster decrease in both quantities compared to the weaker magnetic field, which is to be expected as both the kinetic energy and enstrophy are directly related to the velocity field, and likewise for magnetic energy and j^2 with the magnetic field. Cross helicity for the simulation was not largely affected by the increase in b_0. The MATLAB solver also saw only small changes, with the exception of the run with $\sigma = 0.4$, where the non-normalised quantity decreased significantly more quickly. The plots can be in appendix B.

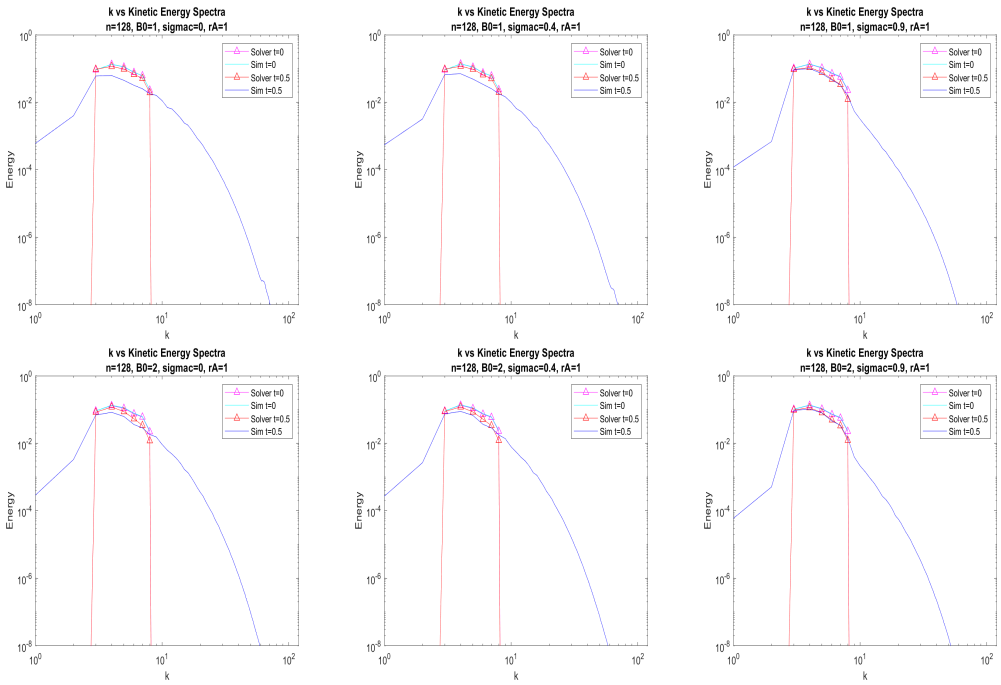

Figure 3.27: Kinetic spectra plots for various initial values of σ_c, comparing $b_0 = 1.0$ with $b_0 = 2.0$

There is not a large influence of b_0 on the energy spectra. We see in figure 3.27 that once again, the linear solutions were most affected. Within the initial band there is a clearly larger decrease in energy, though the dissipation within this range is still very limited, so we still see lower energy levels in simulation results, even within this band. In the simulation plots for $b_0 = 2.0$ we actually

see slightly lower energy for wavenumbers outside the initial band at t=0.5, and higher within it. This indicates that when the magnetic field is stronger we see less energy transferred to higher ks. The values plotted are for the kinetic energy spectra, but the results are the same for the magnetic energy as well.

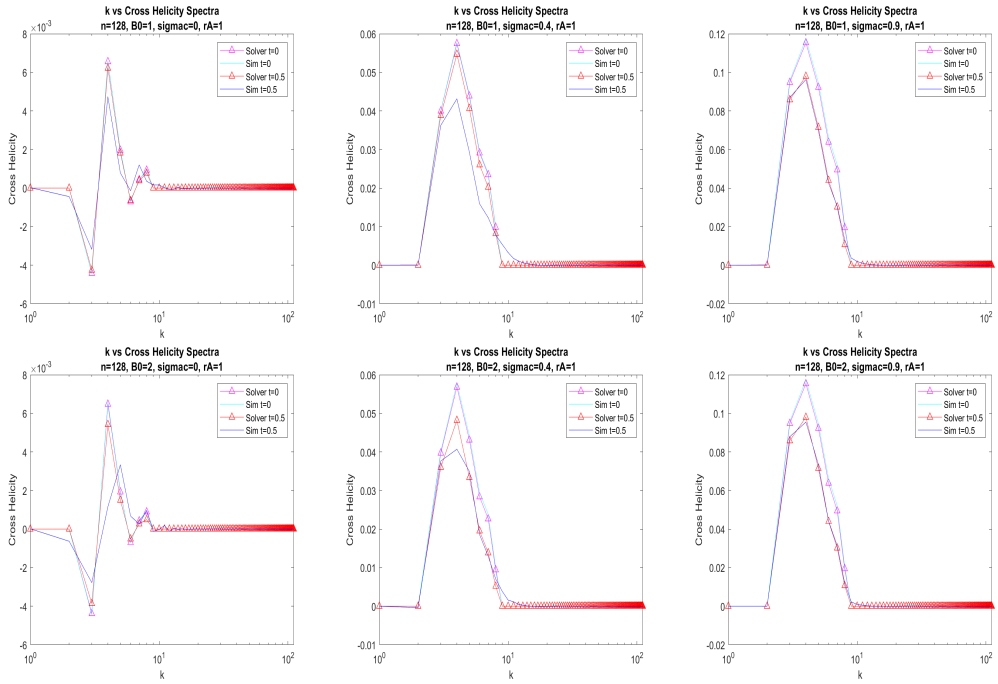

Figure 3.28: Cross helicity spectra plots for various initial values of σ_c, comparing $b_0 = 1.0$ with $b_0 = 2.0$

We see in figure 3.28 that the stronger magnetic field has a significant impact on the cross helicity spectra for lower values of σ_c. The plots for $\sigma_c = 0.9$ were nearly identical for both values of b_0 but for the other tested values of σ_c the cross helicity at t=0.5 was significantly less in the stronger magnetic field for the MATLAB solver. The simulation values when $\sigma_c = 0.4$ are also lower overall when $b_0 = 2.0$, though not as much as with the MATLAB solver. The most intriguing difference is in the simulation values for $\sigma_c = 0.0$. The graph appears to have acquired a sheer relative to the corresponding $b_0 = 1.0$ system. Transfer between scales seems to have happened completely, contributing to a decrease as well as a shift, though I was unable to discern what may have caused this shift.

Chapter 4

Conclusion

4.1 Summary of Project

For this project, I used MATLAB to develop a code that will model the energy levels and associated quantities of the wavelike motions in an MHD fluid. I made use of both my code, and a code provided by my project supervisor, to explore the effects of non-linear turbulent activity in a system, as well as the effects of different starting conditions.

The most significant finding of this exploration was how much more strongly energy is able to dissipate from a turbulent system. The non-linear activity allows for energy to be transferred from larger scales to smaller ones, where the dissipative effects of viscosity and resistivity become significant. I also found that the initial conditions of a system were mostly irrelevant to its long term evolution, in particular the initial Alfvén ratio, which beyond a certain time had no effect on the way the system evolved. Higher values of the initial normalised cross helicity did tend to make the linear solutions more accurately reflect the turbulent solutions. This was shown by direct comparisons between solutions to both the turbulent and wave-like systems which had been given different initial conditions based on variations in their initial Alfvén ratios and initial normalised cross helicities. Apart from the presence of turbulence, the

biggest contributor to variation in the evolution of solutions was the strength of the uniform component to the magnetic field.

There are some obvious areas of extension of these ideas. These are outlined in the following section, but due to the computational limits of my own devices, I was not able to implement them in this project.

4.2 Evaluation and Improvements

A clear and obvious extension of this project would be more extensive use of a higher resolution in the numerical solution to this problem. Due to hardware constraints, I was mostly limited to only working at a resolution of $n = 128^3$, but higher resolutions not only provide more accurate solutions to the differential equations at the expense of more computational power, but they allow for more interactions and transfer of energy between shells in the various spectra.

It would also clearly have been more convenient to have successfully implemented my own solver in the case of a compressible MHD fluid, but I was unfortunately unable to find a solution which could run in a reasonable amount of time at high enough resolutions. Having this would have allowed me to explore the incompressible behaviours and draw comparisons between the wave-like and turbulent behaviour which we saw in the incompressible case was the greatest source of difference between various systems. Most physical systems occur in compressible fluids, so findings would have been more applicable had I been able to achieve it.

Secondly, this project focuses only on the standard MHD equations and systems. As we saw in chapter 2, the MHD equations are formed partially from Ohm's law. Due to the fact that in general conducting fluids always move, the generalised form of Ohm's law was used rather than the ideal form. But none

of the various refining terms were considered. Principal among these neglected terms is the Hall term. The effects of Hall MHD is a natural extension of the scope of this project

Appendices

Appendix A

A Note on Pressure and Linearisation

In section 2.2.1 we referred to the linearisation of the MHD equations and how this process coupled with the divergence operator to make the pressure of the system irrelevant. In this appendix we will look more closely at how this is true. Consider equation (2.11) once more:

$$\begin{aligned} & \frac{\partial \rho}{\partial t} + \nabla \cdot (\rho \boldsymbol{v}) = 0 \\ \implies & \frac{\partial \rho}{\partial t} + \rho \nabla \cdot \boldsymbol{v} + \boldsymbol{v} \cdot \nabla \rho = 0 \\ \implies & \frac{\partial \rho}{\partial t} + \boldsymbol{v} \cdot \nabla \rho = -\rho \nabla \cdot \boldsymbol{v} \end{aligned}$$

Since we are dealing with an incompressible fluid, the left hand side here is zero, hence

$$0 = -\rho \nabla \cdot \boldsymbol{v}$$

in which case either one of rho and $\nabla \cdot \boldsymbol{v}$ must be zero. As this cannot be ρ we therefore have, in the incompressible case, $\nabla \cdot \boldsymbol{v} = 0$

Now, recall the simplified system we began with:

$$\frac{\partial \boldsymbol{v}}{\partial t} + \boldsymbol{v} \cdot \nabla \boldsymbol{v} = -\nabla \left(\frac{P}{\rho_0} + (\boldsymbol{b} + \boldsymbol{b}_0)^2 \right) + (\boldsymbol{b} + \boldsymbol{b}_0) \cdot \nabla \boldsymbol{b} \tag{A.1}$$

$$\frac{\partial \boldsymbol{b}}{\partial t} + \boldsymbol{v} \cdot \nabla \boldsymbol{b} = (\boldsymbol{b} + \boldsymbol{b}_0) \cdot \nabla \boldsymbol{v} \tag{A.2}$$

$$\nabla \cdot \boldsymbol{v} = \nabla \cdot \boldsymbol{b} = 0 \tag{A.3}$$

When we apply the divergence operator to equation (A.1) (and use simplification $P_* = \frac{P}{\rho_0} + (\boldsymbol{b} + \boldsymbol{b}_0)^2$) we obtain

$$\frac{\partial}{\partial t}(\nabla \cdot \boldsymbol{v}) + \nabla \cdot (\boldsymbol{v} \cdot \nabla \boldsymbol{v}) = -\nabla^2 P_* + \nabla \cdot (\boldsymbol{b} \cdot \nabla \boldsymbol{b} + \boldsymbol{b}_0 \cdot \nabla \boldsymbol{b}) \tag{A.4}$$

and since $\nabla \cdot \boldsymbol{v} = 0$, this leaves us with

$$\nabla^2 P_* = \nabla \cdot (\boldsymbol{b} \cdot \nabla \boldsymbol{b} + \boldsymbol{b}_0 \cdot \nabla \boldsymbol{b}) - \nabla \cdot (\boldsymbol{v} \cdot \nabla \boldsymbol{v}) \tag{A.5}$$

So we see the total pressure only has dependence on the non-linear terms in the equation.

Appendix B

Additional Plots

There are some occasions throughout this thesis where it was deemed unnecessary to provide certain outputs as they did not themselves merit much comment, yet their implications were still considered valid enough for them to be included in the paper. These plots can be found in this appendix.

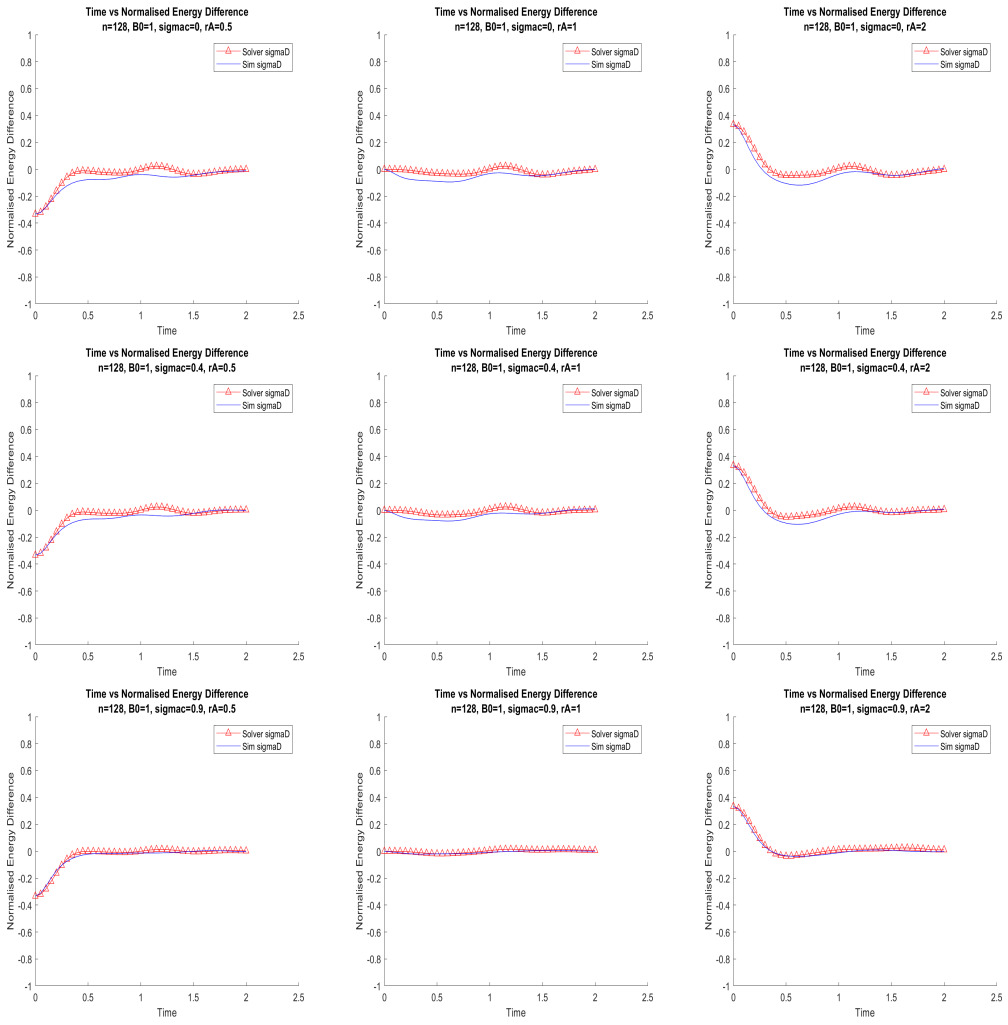

Figure B.1: Plots for the normalised energy difference $\sigma_D = \frac{E_v+E_b}{E_v-E_b}$ for all the tested initial conditions with $b_0 = 1.0$. Note that regardless of initial conditions, σ_D always stabilises around zero

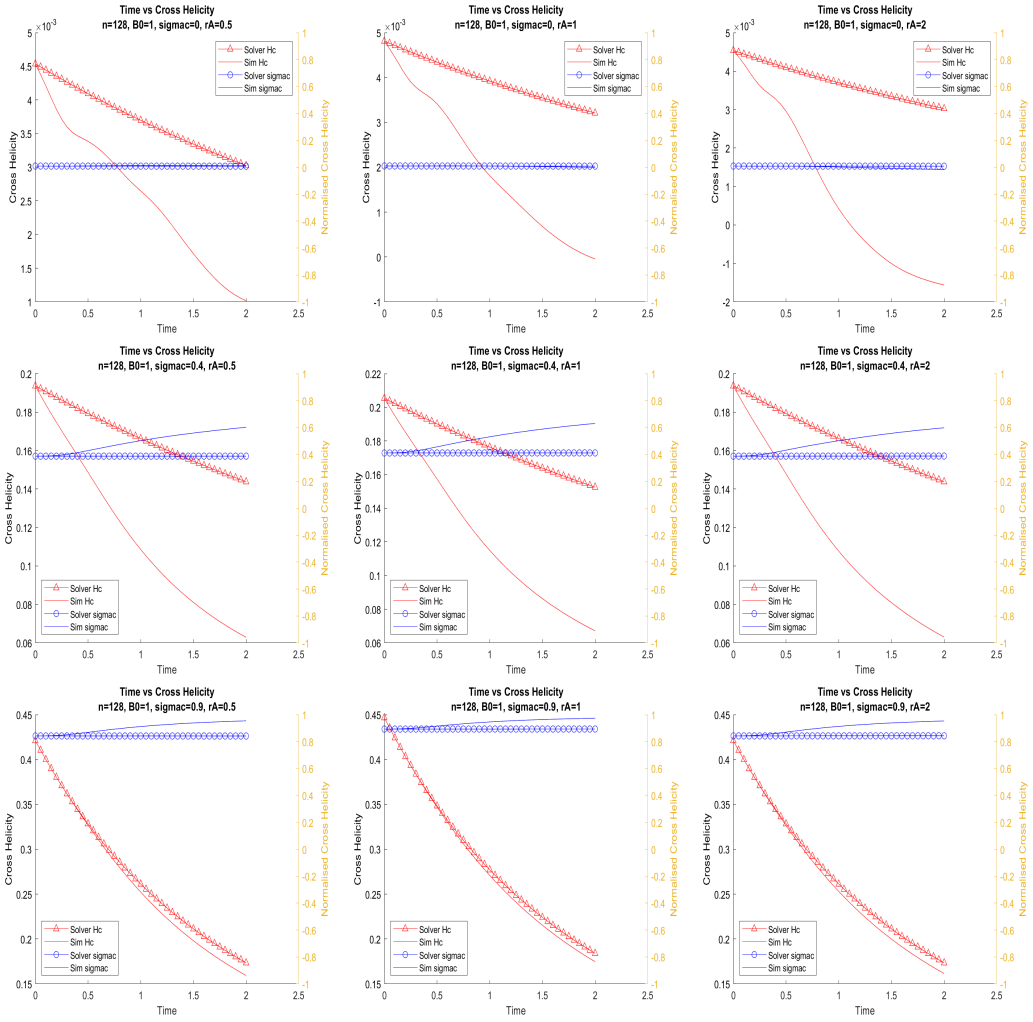

Figure B.2: Plots for the cross helicity H_c and its normalisation σ_c for all the tested initial conditions with $b_0 = 1.0$

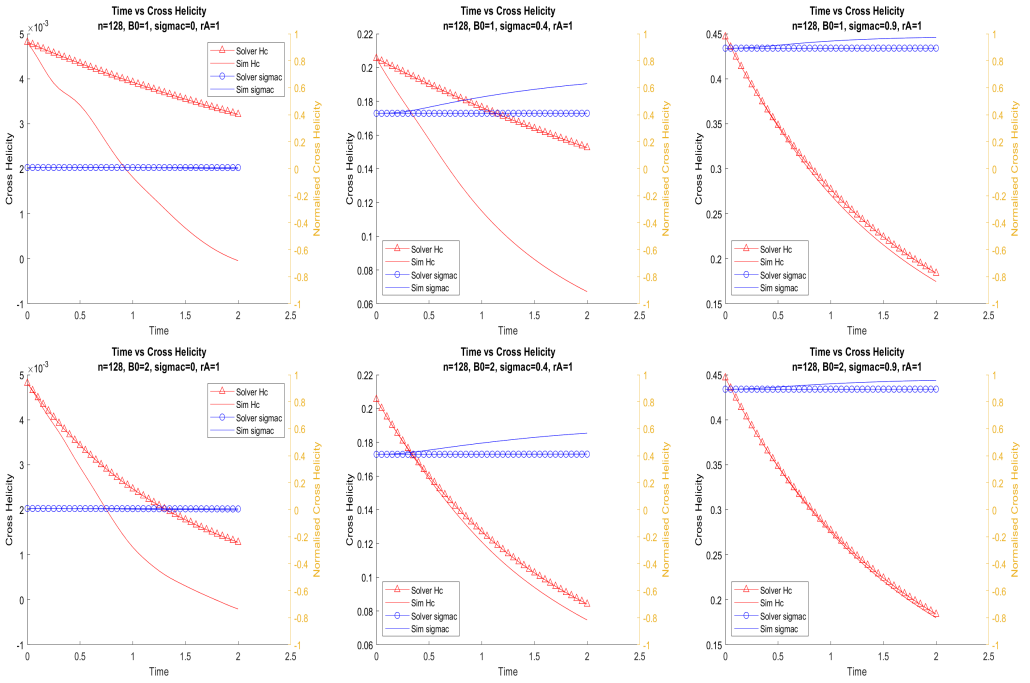

Figure B.3: Cross helicity plots for various initial values of σ_c, comparing $b_0 = 1.0$ with $b_0 = 2.0$

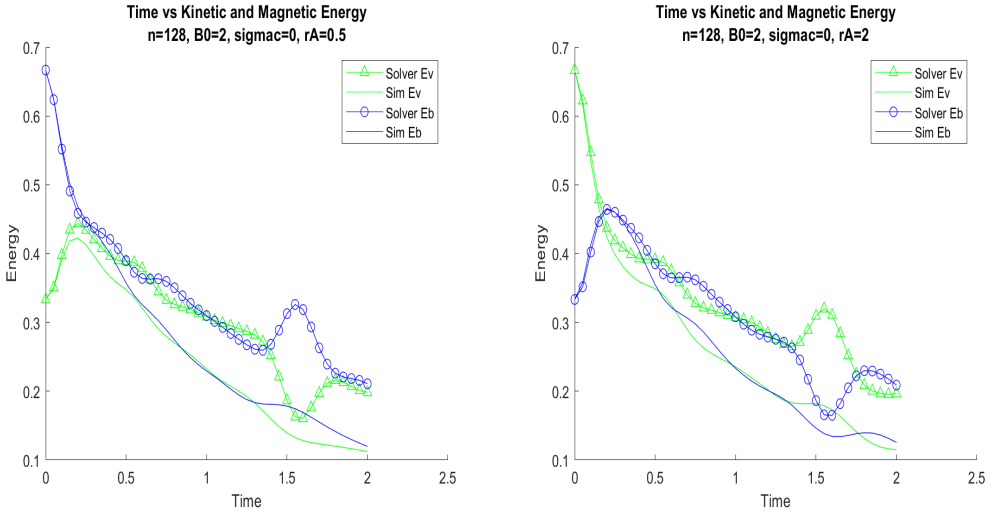

Figure B.4: In the energy plots for $b_0 = 2.0$ and $r_A \neq 1.0$ we see a sudden increase in amplitude of the oscillations with no apparent cause. It would be interesting to investigate further, however I was unfortunately not able to at this time

References

Alfvèn, H. Existence of electromagnetic-hydrodynamic waves. *Nature (London)*, 150(3805):405–406, 1942. ISSN 0028-0836.

Alfvén, Hannes. On the cosmogony of the solar system iii. *Stockholms Observatoriums Annaler*, 14:9–1, 1946.

Allen, T.K., Baker, William R., Pyle, Robert V., and Wilcox, John M. Experimental generation of plasma alfven waves. *Physical review letters*, 2(9): 383–384, 1959. ISSN 0031-9007.

El-Alaoui, Mostafa, Walker, Raymond J., Weygand, James M., Lapenta, Giovanni, and Goldstein, Melvyn L. Magnetohydrodynamic turbulence in the earth's magnetotail from observations and global mhd simulations. *Frontiers in Astronomy and Space Sciences*, 8, 2021. ISSN 2296-987X. doi: 10.3389/fspas.2021.620519.

Elsässer, Walter M. The hydromagnetic equations. *Physical review*, 79(1): 183–183, 1950. ISSN 0031-899X.

Frisch, U. *Turbulence: The Legacy of A. N. Kolmogorov*. Cambridge University Press, 1995. ISBN 9781139935975.

Galtier, Sébastien. *Introduction to Modern Magnetohydrodynamics*. Cambridge University Press, 2016.